

## Supporting Information

### **Designing Highly Stable Coordination-Driven Metallacycle for**

### **Imaging-Guided Photodynamic Cancer Theranostics**

Lizhen He,<sup>#b</sup> Li-Xuan Cai,<sup>#a</sup> Meng-Hua Li,<sup>c</sup> Guang-Lu Zhang,<sup>a</sup> Li-Peng Zhou,<sup>a</sup> Tianfeng Chen,<sup>\*b</sup>  
Mei-Jin Lin,<sup>\*c</sup> Qing-Fu Sun<sup>\*a</sup>

<sup>a</sup> State Key Laboratory of Structural Chemistry, Fujian Institute of Research on the Structure of Matter, Chinese Academy of Sciences, Fuzhou 350002, China

<sup>b</sup> Department of Chemistry, Jinan University, Guangzhou 510632, China

<sup>c</sup> State Key Laboratory of Photocatalysis on Energy and Environment, College of Chemistry, Fuzhou University, Fuzhou 350116, China

\*Corresponding email: qfsun@fjirsm.ac.cn; tchentf@jnu.edu.cn; meijin\_lin@fzu.edu.cn

# Lizhen He and Li-Xuan Cai contributed equally.

## Contents

### Section A. General

### Section B. Synthesis and characterization of compounds

- 1. Synthesis of N, N'-bis (3, 5-dimethyl-pyrazole)-1, 6, 7, 12-tetrachloroperylene-3, 4, 9, 10-tetracarboxy diimide (**S1**)
- 2. Synthesis of N, N-bis(3,5-dimethyl-pyrazole)- 1,6,7,12-(4-(tert-butyl)phenoxy)-perylene-3, 4, 9, 10-tetracarboxy diimide (**1**)
- 3. Synthesis of N-(n-butyl)-N'-(3, 5-dimethyl-pyrazole)-1, 6, 7, 12-tetrachloroperylene-3, 4, 9, 10-tetracarboxy diimide (**S2**)
- 4. Synthesis of N-(n-butyl)-N'-(3, 5-dimethyl-pyrazole) - 1, 6, 7, 12-(4-(tert-butyl) phenoxy)-3, 4, 9, 10-tetracarboxy diimide (**3**)
- 5. Synthesis of metallacycle **2**
- 6. Synthesis of complex **4**.
- 7. Single crystal X - ray diffraction study

### Section C. Photophysical properties and singlet oxygen production

- 1. Photophysical data for all compounds **1-4**.
- 2.  $^1\text{O}_2$  generation of all compounds in DMSO solution

### Section D. Stability, Bio-Imaging and Photodynamic Therapy

- 1. Stability of metallacycle **2** in aqueous media
- 2. Cell culture and MTT assay
- 3. Flow Cytometric Analysis
- 4. Measurement of singlet oxygen generation ( $^1\text{O}_2$ ) in HeLa cells triggered by metallacycle **2** and PDT
- 5. Real-time living cell imaging
- 6. Cell distribution of metallacycle **2**
- 7. Cell localization of metallacycle **2**
- 8. *In vivo* fluorescence imaging of metallacycle **2**

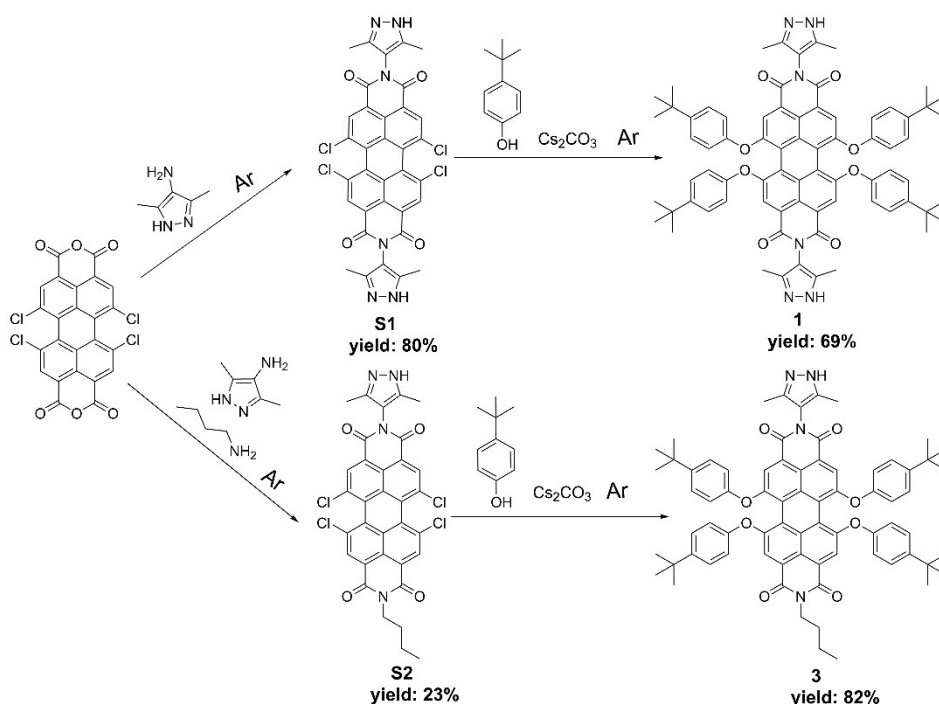
- 9. *In vitro* biocompatibility and safety evaluation of metallacycle **2**
- 10. *In vitro* cellular uptake of metallacycle **2**

## Section E. References

### Section A. General

All chemicals and solvents were purchased from commercial sources and used as supplied without further purification unless otherwise noted. Perylene 3,4,9,10-tetracarboxylic acid dianhydride (PTCDA, 98%), propionic acid (analytical reagent grade), dimethylformamide (DMF, analytical reagent grade), N-methyl-2-pyrrolidone (NMP, analytical reagent grade), 4-tert-butylphenol (analytical reagent grade), *n*-butylamine (analytical reagent grade) and Cs<sub>2</sub>CO<sub>3</sub> (analytical reagent grade) were obtained from the commercial suppliers. 1, 6, 7, 12-Tetrachloroperylene-3, 4, 9, 10-tetracarboxylic dianhydride<sup>[S1]</sup> and 4-amino-3,5-di-methyl-pyrazole<sup>[S2]</sup> were prepared according to the literatures. Deuterated solvents were purchased from Sigma-Aldrich and J&K scientific. 1D and 2D NMR spectra were conducted on a Bruker BioSpin AVANCE III 400 or a JEOL JNM-ECZ400S/L1 NMR spectrometer. The NMR chemical shifts ( $\delta$ ) are reported in ppm (parts per million) with respect to either the internal tetramethylsilane (TMS) or solvent residue signals. The UV-Vis spectra were measured on UV-2700 from Shimadzu or Perkin-Elmer Lambda 950 spectrometers. Electro-spray-ionization time-of-flight mass spectroscopy (ESI-TOF-MS) of complexes were recorded on Impact II UHR-TOF mass spectrometry from Bruker, with tuning mix as the internal standard. ESI-MS spectra of ligands and precursors were recorded on Exactive Plus mass spectrometry from Thermo Fisher Scientific. Luminescence spectra and photoluminescence quantum yields were measured on a FS5 from Edinburgh Instruments Ltd with an integration sphere.

### Section B. Synthesis and characterization of compounds



**Scheme S1.** Synthesis route for precursors **S1**, **S2** and ligands **1** and **3**.

### 1. Synthesis of *N,N'*-bis(3,5-dimethyl-1*H*-pyrazole-4-yl)-1,6,7,12-tetrachloroperylene-

**3,4,9,10-tetracarboxy diimide (S1).** 4-Amino-3,5-dimethylpyrazole (1.048 g, 9.44 mmol) was added to a mixture of 1,6,7,12-tetrachloroperylene-3,4,9,10-tetracarboxylic dianhydride (0.996 g, 1.88 mmol) and propionic acid (20 mL) under argon atmosphere. The reaction mixture was stirred and heated at 140 °C for 24 h. After being cooled to room temperature, the resultant precipitate was filtered and washed with deionized water until the filtrate became neutral. The crude product was purified by silica gel column chromatography with petroleum ether (PE) and dichloromethane (DCM) (from 3:1 to 1:10 v/v) to give product **S1** as a red solid 1.077 g (1.50 mmol, 80% yield). <sup>1</sup>H NMR (400 MHz, DMSO-*d*<sub>6</sub>) δ 12.50 (s, 2H), 8.64 (s, 4H), 2.05 (s, 12H). <sup>13</sup>C NMR (100 MHz, CF<sub>3</sub>COOD) δ 163.40, 145.80, 136.91, 134.76, 131.58, 130.60, 123.78, 121.76, 115.12, 8.28. ESI-MS: *m/z* calculated for [C<sub>34</sub>H<sub>18</sub>Cl<sub>4</sub>N<sub>6</sub>O<sub>4</sub>-H]<sup>-</sup> 714.0138, found 714.0163.

### 2. Synthesis of *N,N'*-bis(3,5-dimethyl-1*H*-pyrazole-4-yl)-1,6,7,12-(4-(*tert*-butyl)phenoxy)-

**perylene-3,4,9,10-tetracarboxylic diimide (1).** *N,N'*-bis(3,5-dimethyl-pyrazole)-1,6,7,12-tetrachloroperylene-3,4,9,10-tetracarboxy diimide (0.215 g, 0.30 mmol), 4-*t*-butylphenol (0.270 g, 1.80 mmol) and Cs<sub>2</sub>CO<sub>3</sub> (0.616 g, 1.90 mmol) were suspended in NMP (10 mL) and stirred under argon atmosphere at 100 °C for 3 h. After being cooled to room temperature, the reaction mixture was dropped into 1 N HCl (200 mL) under stirring. The solid was separated by filtration, and then washed successively with deionized water (3 × 30 mL) and methanol (3 × 30 mL). The crude

product was purified by silica gel column chromatography with PE and DCM (from 5:1 to 1:3 v/v) to give ligand **1** as a dark red solid (0.246 g, 0.21 mmol, 69% yield). <sup>1</sup>H NMR (400 MHz, DMSO-*d*<sub>6</sub>) δ 12.38 (s, 2H), 7.94 (s, 4H), 7.32 (d, *J* = 7.8 Hz, 8H), 6.91 (d, *J* = 7.8 Hz, 8H), 1.94 (s, 6H), 1.87 (s, 6H), 1.25 (s, 36H). <sup>13</sup>C NMR (100 MHz, CF<sub>3</sub>COOD) δ 166.12, 159.41, 154.98, 151.66, 147.70, 135.54, 129.13, 124.55, 123.75, 122.85, 121.98, 121.36, 117.18, 36.07, 32.34, 10.15. ESI-MS *m/z* calculated for [C<sub>74</sub>H<sub>70</sub>N<sub>6</sub>O<sub>8</sub>-H]<sup>-</sup> 1170.5250, found 1170.5304.

### 3. Synthesis of N-(*n*-butyl)-N'-(3, 5-di-methyl-pyrazole)-1, 6, 7, 12-tetrachloroperylene-3, 4, 9, 10-tetracarboxy diimide (S2)

1,6,7,12-tetrachloroperylene-3,4,9,10-tetracarboxylic dianhydride (2.120 g, 4.00 mmol) and 4-amino-3,5-dimethyl-pyrazole (0.450 g, 4.05 mmol) was dissolved in toluene (50 mL) in a two-necked flask. Under argon atmosphere, *n*-butylamine (0.5 mL, 5 mmol) was added to the system. The mixture was first stirred at room temperature for 30 min and then at 110 °C for 12 h. After being cooled to room temperature, the toluene solvent was removed under reduced pressure. The solid obtained was washed with deionized water until the filtrate became neutral. The crude product was purified by silica gel column chromatography with PE and DCM (from 3:1 to 1:5 v/v) to give product **S2** as a red solid (0.624g, 0.92 mmol, 23% yield). <sup>1</sup>H NMR (400 MHz, CDCl<sub>3</sub>): δ 8.74 (s, 2H), 8.71 (s, 2H), 4.23 (t, *J* = 7.4 Hz, 2H), 2.19 (s, 6H), 1.75 (m, 2H), 1.48 (m, 2H), 1.01 (t, *J* = 7.2 Hz, 3H). <sup>13</sup>C NMR (100 MHz, CDCl<sub>3</sub>) δ 162.24, 161.73, 135.58, 135.42, 133.49, 132.99, 132.74, 131.63, 131.51, 129.05, 128.48, 123.69, 123.41, 123.10, 40.77, 30.18, 20.34, 13.84, 10.76. ESI-MS: *m/z* calculated for [C<sub>33</sub>H<sub>20</sub>Cl<sub>4</sub>N<sub>4</sub>O<sub>4</sub>-H]<sup>-</sup> 678.0204, found 678.0222.

### 4. Synthesis of N-(*n*-butyl)-N'-(3, 5-di-methyl-pyrazole) - 1, 6, 7, 12-(4-(*tert*-butyl)phenoxy)-3,4,9,10-tetracarboxy diimide (3)

N-(*n*-butyl)-N'-(3, 5-di-methyl-pyrazole)-1, 6, 7, 12-tetrachloroperylene-3, 4, 9, 10-tetracarboxy diimide (0.400 g, 0.59 mmol), 4-*t*-butylphenol (0.496 g, 3.33 mmol) and Cs<sub>2</sub>CO<sub>3</sub> (1.238 g, 3.80 mmol) were added into DMF (40 mL) and the suspension was stirred under argon atmosphere at 100 °C for 3 h. After being cooled to room temperature, the reaction mixture was dropped into 1 N HCl (400 mL) under stirring. The solid was separated by filtration, and then washed successively with water (3 × 30 mL) and methanol (3 × 30 mL). The crude product was purified by silica gel column chromatography with PE and DCM (from 5:1 to 1:2 v/v) to give ligand **3** as a dark red solid (556 mg, 0.49 mmol, 82% yield). <sup>1</sup>H NMR (400 MHz, CF<sub>3</sub>COOD) δ 8.35 (s, 2H), 8.24 (s, 2H), 7.39 (d, *J* = 8.6 Hz, 4H), 7.36 (d, *J* = 8.6 Hz, 4H), 6.94 (d, *J* = 8.6 Hz, 4H), 6.88 (d, *J* = 8.6 Hz, 4H), 4.08 (br, 2H), 2.37 (s, 6H), 1.59 (m, 2H), 1.40 (m, 2H), 1.37 (s, 18H), 1.35 (s, 18H), 0.95 (t, *J* = 7.2 Hz, 3H). <sup>13</sup>C NMR (100 MHz, CF<sub>3</sub>COOD) 167.61, 166.60, 159.08, 154.88, 154.60, 151.38, 151.16, 147.74, 135.07, 134.72, 128.99, 128.93, 124.99, 123.68, 123.58, 123.52, 123.24, 122.14, 121.95, 121.37, 121.12, 121.08, 117.43, 43.66, 36.14, 36.10, 32.39, 32.30, 31.54, 21.85,

14.27, 10.25. ESI-TOF-MS:  $m/z$  calculated for  $[C_{73}H_{72}N_4O_8+H]^+$  1133.5423, found 1133.5461.

**5. Synthesis of metallacycle 2.** Ligand **1** (11.7 mg, 10.0  $\mu$ mol) was treated with  $BpyPd(NO_3)_2$  (7.16 mg, 19.0  $\mu$ mol) in DMSO (1 mL) at 90 °C for 10 h. A homogeneous dark-red solution was obtained and  $^1H$  NMR confirmed the quantitative formation of  $(Bpy)_8Pd_8(1-2H)_4 \cdot (NO_3)_8$  (**2**).  $^1H$  NMR (400 MHz, DMSO- $d_6$ )  $\delta$  8.77 (br, 4H), 8.48 (br, 4H), 8.09 (br, 4H), 7.95 (br, 4H), 7.88 (br, 4H), 7.41 (br, 8H), 7.03 (br, 8H), 2.23 (br, 12H), 1.33 (br, 36H).  $^{13}C$  NMR (100 MHz, DMSO- $d_6$ )  $\delta$  162.58, 162.16, 157.17, 156.01, 155.77, 153.09, 149.76, 147.61, 147.46, 143.04, 133.12, 128.68, 127.28, 125.15, 123.87, 123.50, 120.03, 119.73, 119.36, 114.68, 34.68, 34.59, 31.71, 31.61, 12.66. ESI-TOF-MS:  $m/z$  calculated for  $[M-8 \cdot NO_3]^{8+}$  847.2290, found 847.2290.

**6. Synthesis of complex 4.** Ligand **3** (11.3 mg, 10.0  $\mu$ mol) was treated with  $BpyPd(NO_3)_2$  (4.30 mg, 11.0  $\mu$ mol) in DMSO (1 mL) at 90 °C for 10 h. A homogeneous dark-red solution was obtained and  $^1H$  NMR spectrum confirmed the quantitative formation of  $(Bpy)_2Pd_2(3-2H)_2 \cdot (NO_3)_2$  (**4**).  $^1H$  NMR (400 MHz, DMSO- $d_6$ )  $\delta$  8.73 (br, 2H), 8.46 (br, 2H), 7.91 (br, 8H), 7.32 (br, 8H), 6.88 (br, 8H), 3.93 (br, 2H), 2.19 (br, 6H), 1.54 (br, 2H), 1.24 (br, 38H), 0.87 (t,  $J = 7.2$  Hz, 3H).  $^{13}C$  NMR (100 MHz, DMSO- $d_6$ )  $\delta$  162.58, 161.94, 157.20, 155.73, 152.97, 152.73, 150.06, 147.49, 147.37, 143.05, 132.88, 132.67, 128.61, 127.11, 126.92, 126.66, 125.07, 122.94, 119.92, 119.78, 119.69, 119.15, 114.71, 34.96, 34.62, 34.55, 34.46, 34.41, 31.67, 31.60, 31.52, 31.48, 29.58, 22.55, 20.27, 14.09. ESI-TOF-MS:  $m/z$  calculated for  $[M-2 \cdot NO_3]^{2+}$  1394.5022 found 1394.5089.

## 7. Single crystal X-ray diffraction study

The X-ray diffraction study for metallacycle **2** was carried out at a SuperNova Dual Source diffractometer from Agilent Technologies, using the Cu source. Data reduction was performed with the CrysAlisPro package.<sup>[S3]</sup> The structure was solved by direct method and refined by full-matrix least-squares on  $F^2$  with anisotropic displacement using the SHELX software package.<sup>[S4]</sup> Some of solvent molecules were highly disordered and could not be reasonably located. These residual intensities were removed by PLATON/SQUEEZE routine.<sup>[S5]</sup>

Crystal data for **2**: Space group  $P-1$ ,  $a = 22.2838(7)$  Å,  $b = 27.0021(9)$  Å,  $c = 29.9657(6)$  Å,  $V = 16907.2(9)$  Å<sup>3</sup>,  $Z = 1$ ,  $T = 293$  K. Anisotropic least-squares refinement on 60159 independent merged reflections ( $R_{int} = 0.1297$ ) converged at residual  $wR2 = 0.2907$  for all data; residual  $R1 = 0.1135$  for 27647 observed data [ $I > 2\sigma(I)$ ], and goodness of fit (GOF) = 0.981.

**Table S1.** Crystal data and structure refinement for metallacycle **2**.

Empirical formula	C408 H400 N48 O64 Pd8
Formula weight	7850.94
Temperature	293 K
Wavelength	1.54184 Å
Crystal system	Triclinic
Space group	<i>P</i> -1
Unit cell dimensions	a = 22.2838(7) Å      α = 87.829(2)° b = 27.0021(9) Å      β = 86.244(2)° c = 29.9657(6) Å      γ = 70.024(3)°
Volume	16907.2(9) Å <sup>3</sup>
Z	1
Density (calculated)	0.771 Mg/m <sup>3</sup>
Absorption coefficient	2.048 mm <sup>-1</sup>
F(000)	4064
Crystal size	0.5 x 0.3 x 0.3 mm <sup>3</sup>
Theta range for data collection	3.405 to 69.198°.
Index ranges	-26 ≤ h ≤ 26, -32 ≤ k ≤ 32, -36 ≤ l ≤ 18
Reflections collected	113024
Independent reflections	60159 [R(int) = 0.1297]
Completeness to theta = 67.684°	97.2 %
Refinement method	Full-matrix least-squares on F <sup>2</sup>
Data / restraints / parameters	60159 / 2312 / 2185
Goodness-of-fit on F <sup>2</sup>	0.981
Final R indices [I > 2σ(I)]	R1 = 0.1135, wR2 = 0.2907

R indices (all data)	R1 = 0.1726, wR2 = 0.3556
Extinction coefficient	n/a
Largest diff. peak and hole	2.066 and -1.112 e.Å <sup>-3</sup>

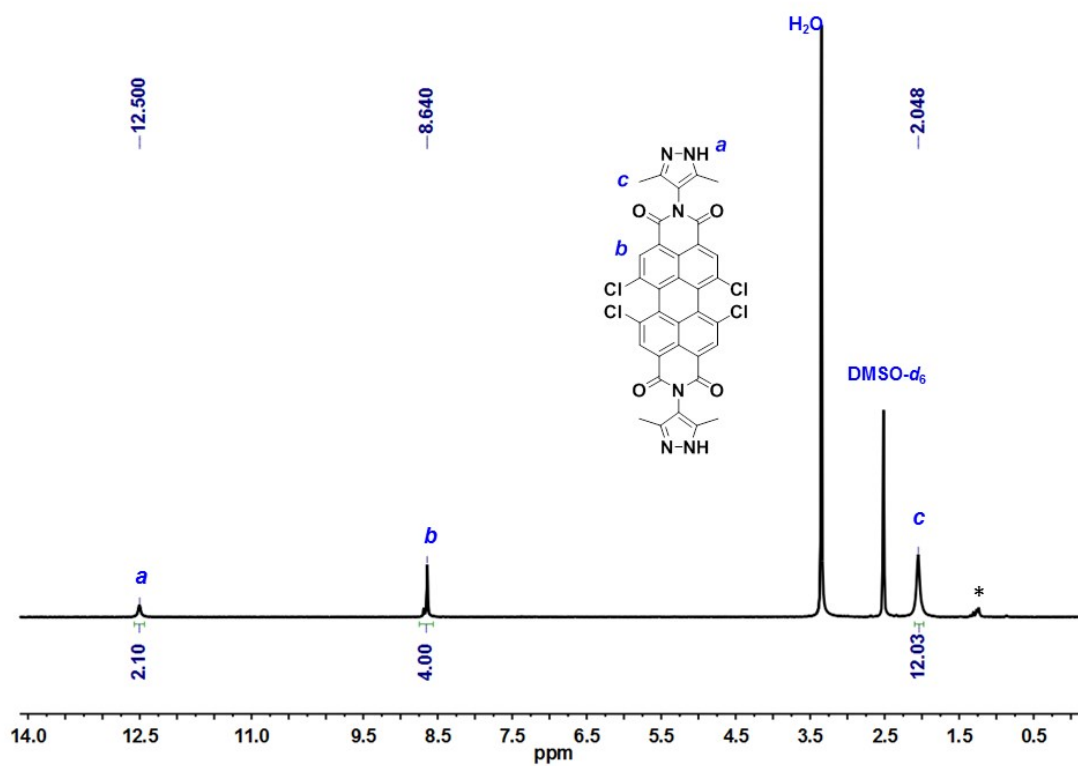


**Figure S1** <sup>1</sup>H NMR spectrum of **S1** (400 MHz, DMSO-*d*<sub>6</sub>, 298 K). Signals labeled with star denote solvent (PE) residue.

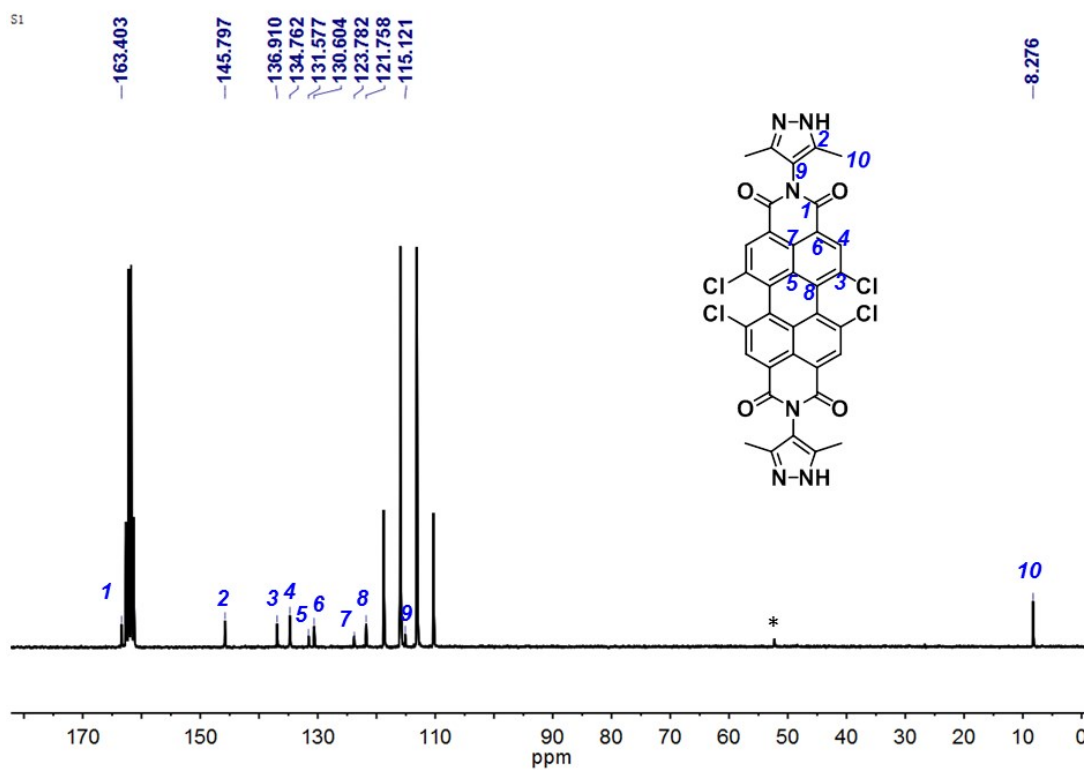


**Figure S2**  $^{13}\text{C}$  NMR spectrum of **S1** (100 MHz,  $\text{CF}_3\text{COOD}$ , 298 K). Signal labeled with star denotes solvent (DCM) residue.

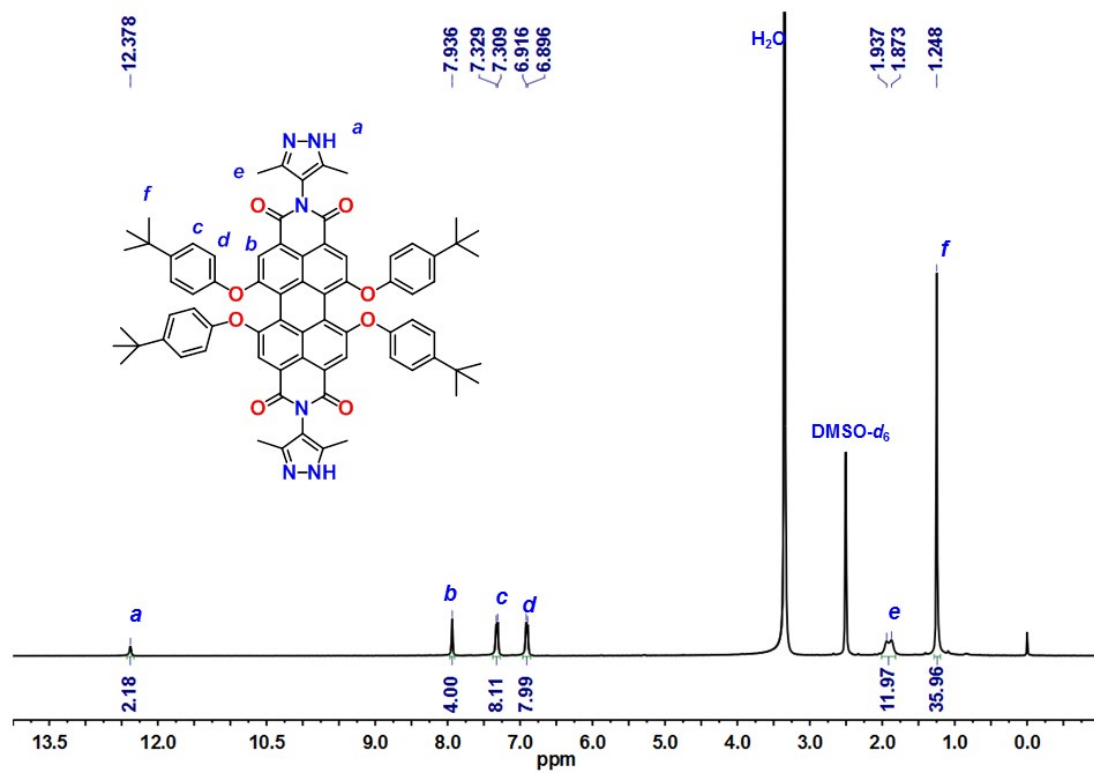


Figure S3  $^1\text{H}$  NMR spectrum of ligand **1** (400 MHz,  $\text{DMSO-}d_6$ , 298 K).

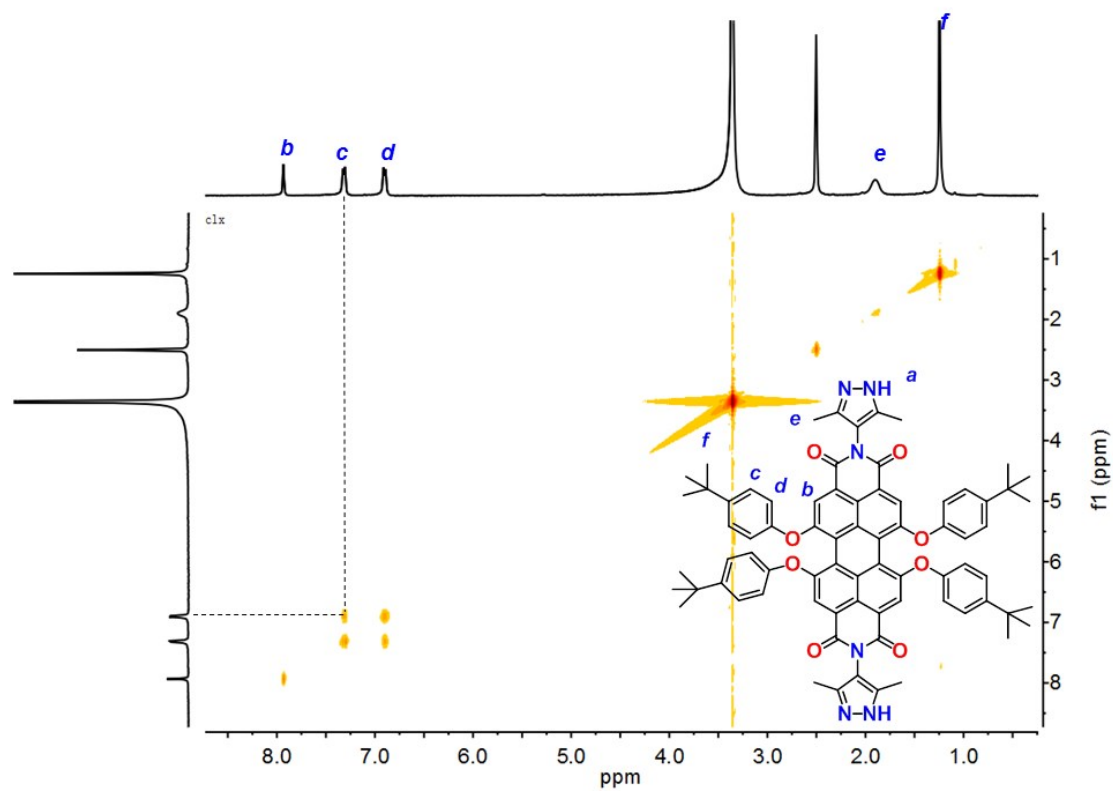
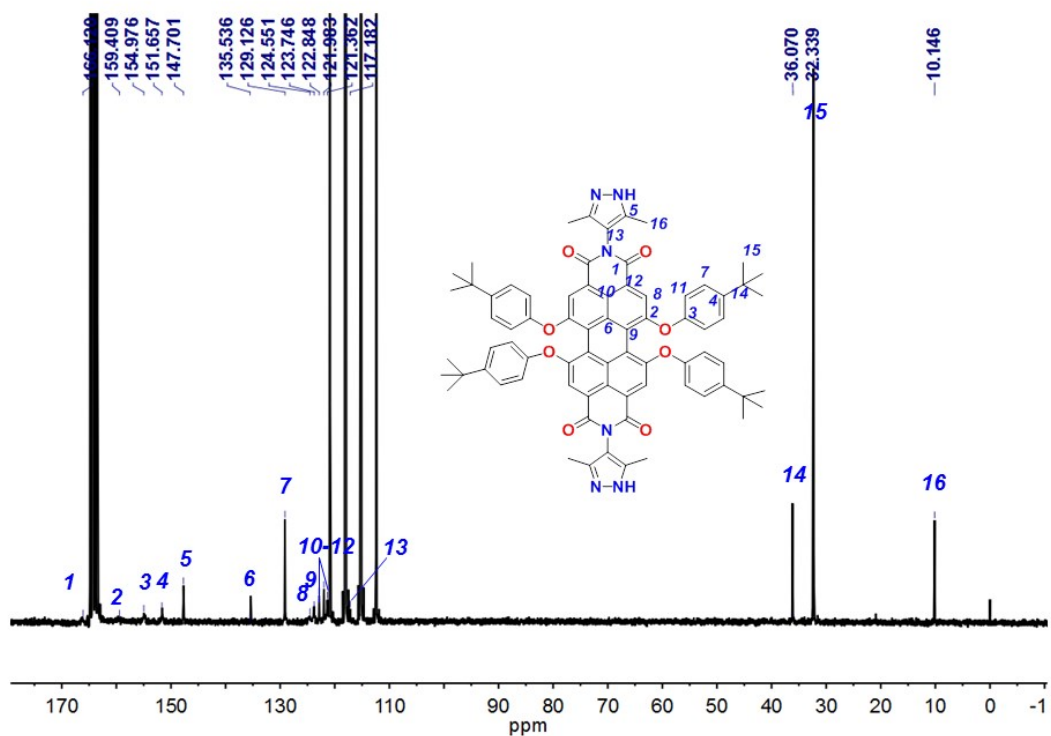


Figure S4  $^1\text{H}$ - $^1\text{H}$  COSY spectrum of ligand **1** (400 MHz,  $\text{DMSO-}d_6$ , 298 K).



**Figure S5**  $^{13}\text{C}$  NMR spectrum of ligand **1** (100 MHz,  $\text{CF}_3\text{COOD}$ , 298 K). The  $^{13}\text{C}$  NMR for this compound is difficult to measure due to its poor solubility, even in  $\text{CF}_3\text{COOD}$ .

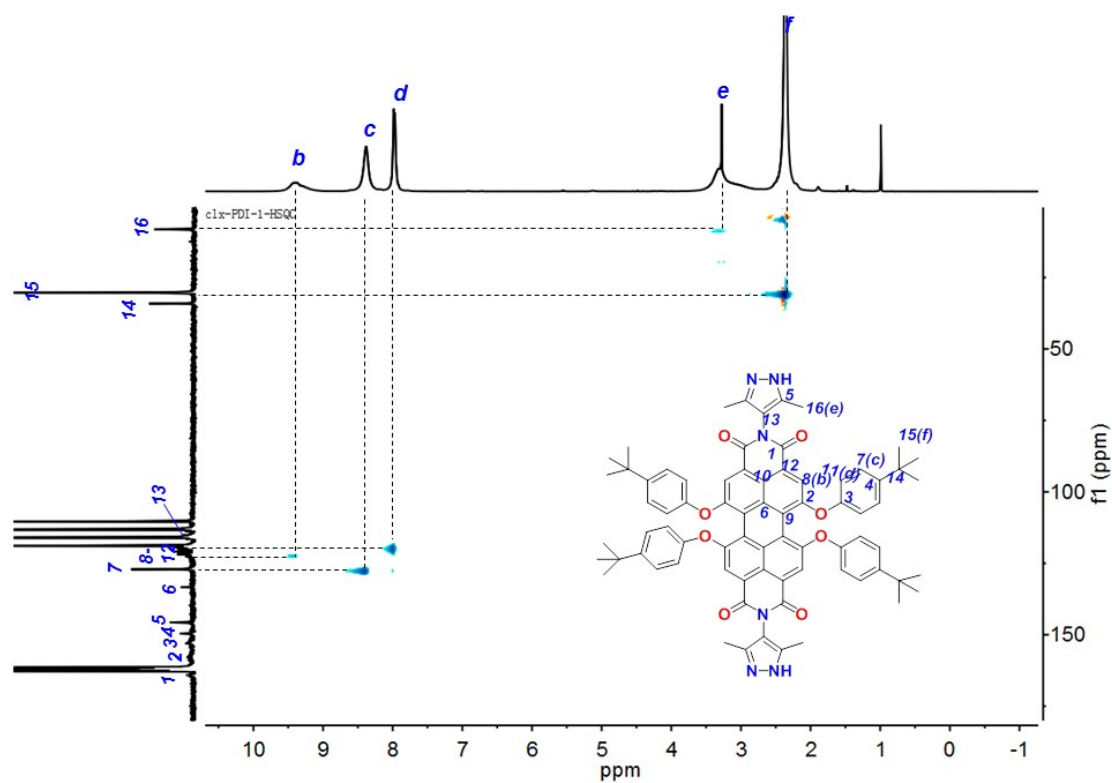


Figure S6  $^1\text{H}$ - $\{^{13}\text{C}\}$  HSQC spectrum of ligand **1** (400 MHz,  $\text{CF}_3\text{COOD}$ , 298 K).

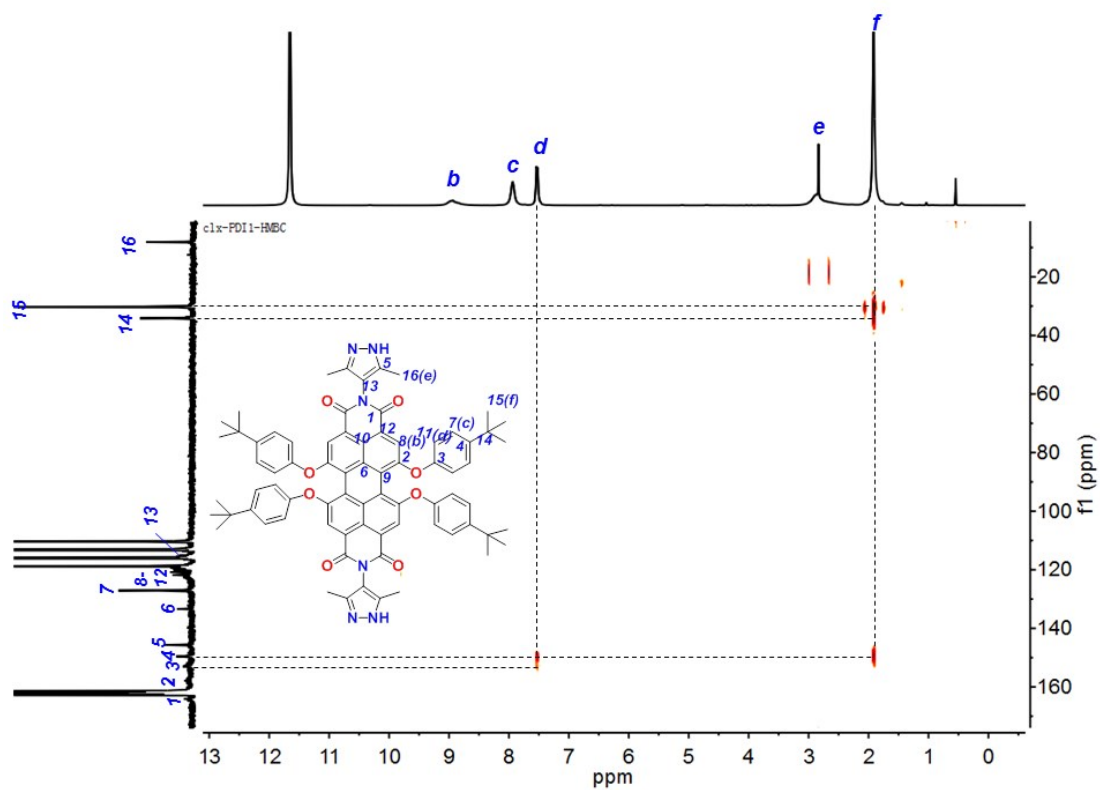
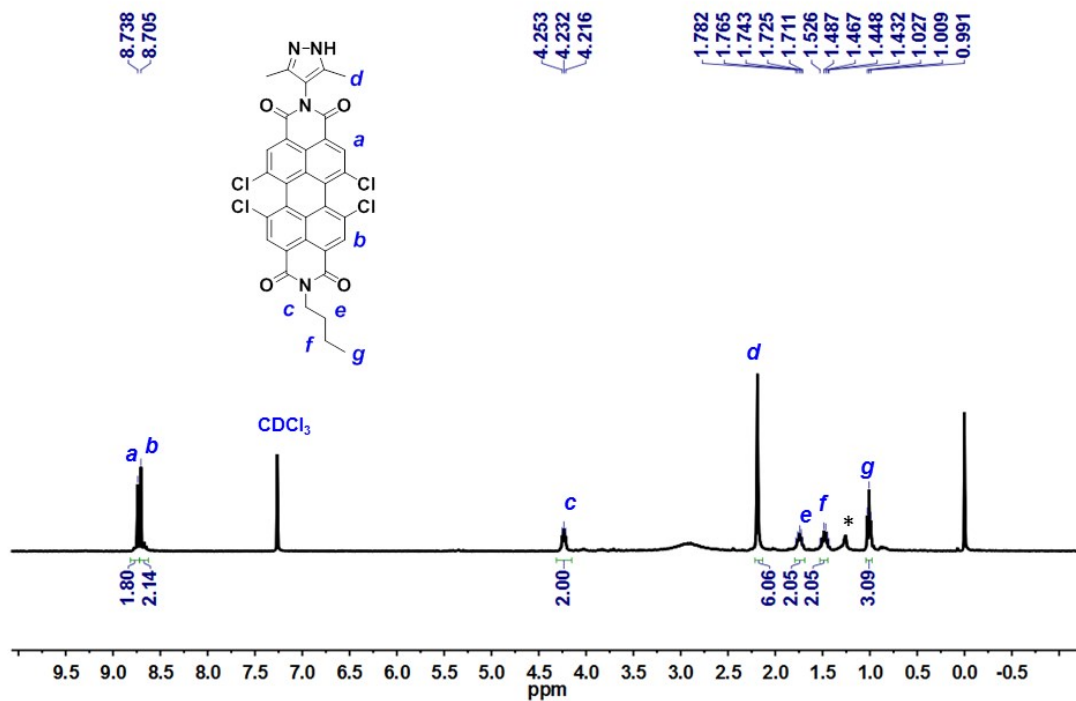
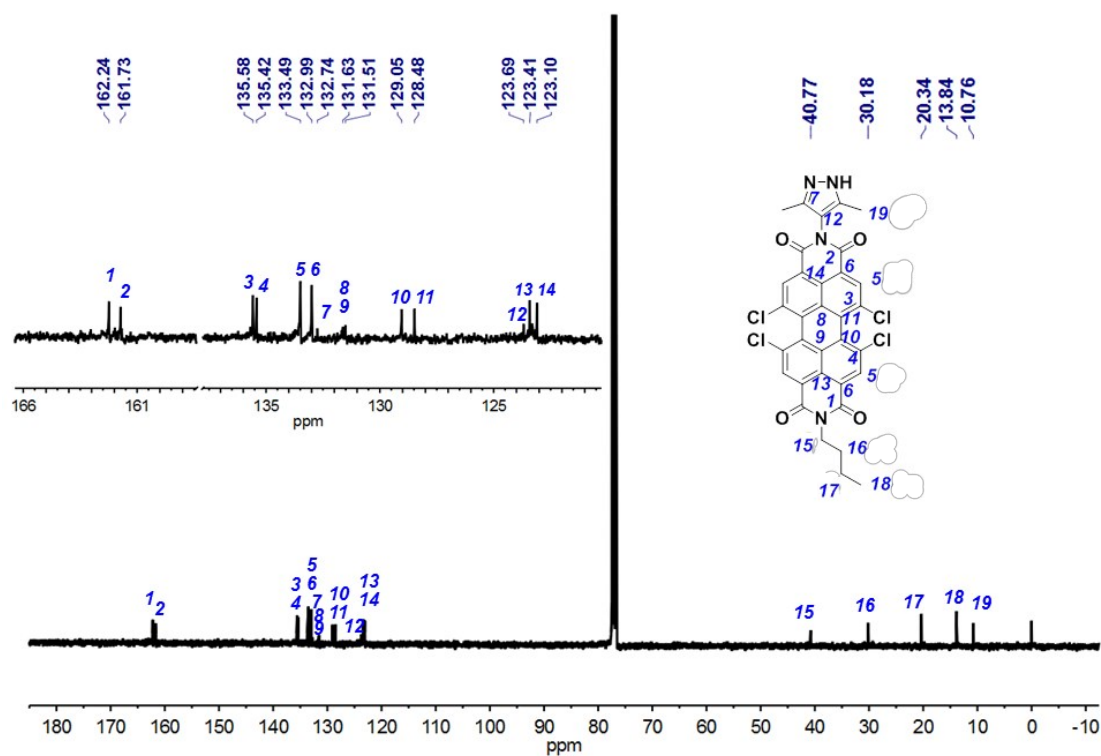


Figure S7  $^1\text{H}$ - $\{^{13}\text{C}\}$  HMBC spectrum of ligand **1** (400 MHz,  $\text{CF}_3\text{COOD}$ , 298 K).



**Figure S8**  $^1\text{H}$  NMR spectrum of S2 (400 MHz,  $\text{CDCl}_3$ , 298 K). Signals labeled with star denote solvent (PE) residue.



**Figure S9**  $^{13}\text{C}$  NMR spectrum of S2 (100 MHz,  $\text{CDCl}_3$ , 298 K).

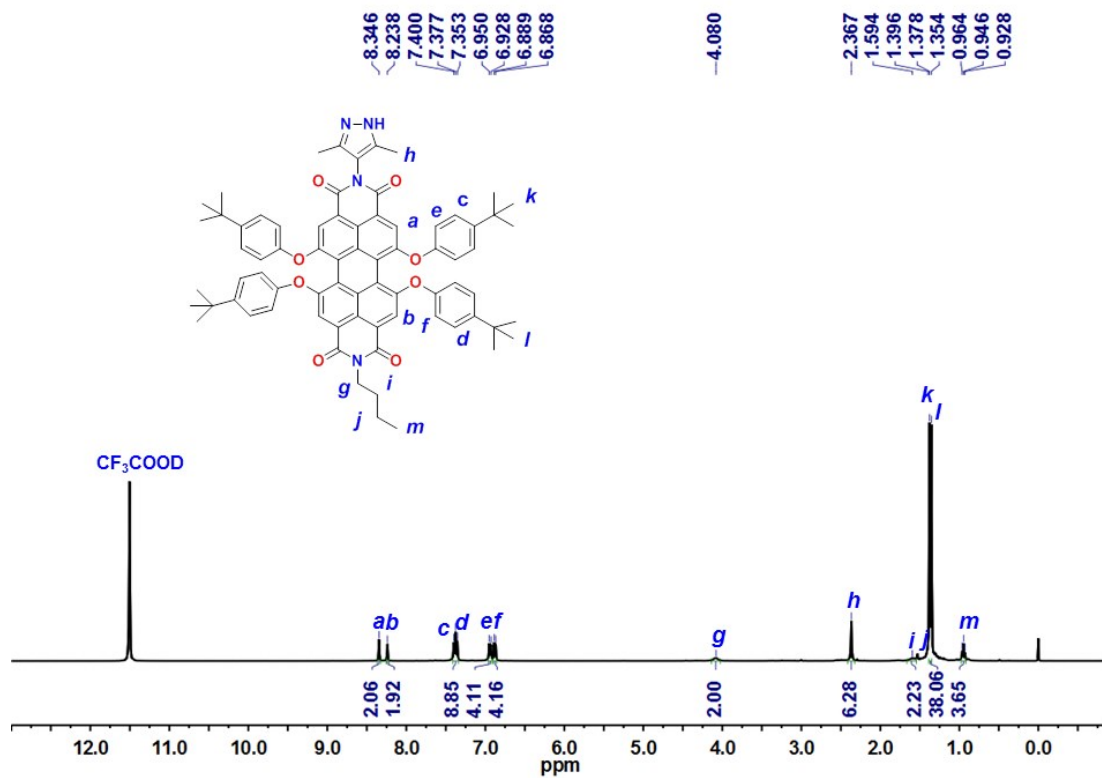


Figure S10 <sup>1</sup>H NMR spectrum of ligand **3** (400 MHz, CF<sub>3</sub>COOD, 298 K).

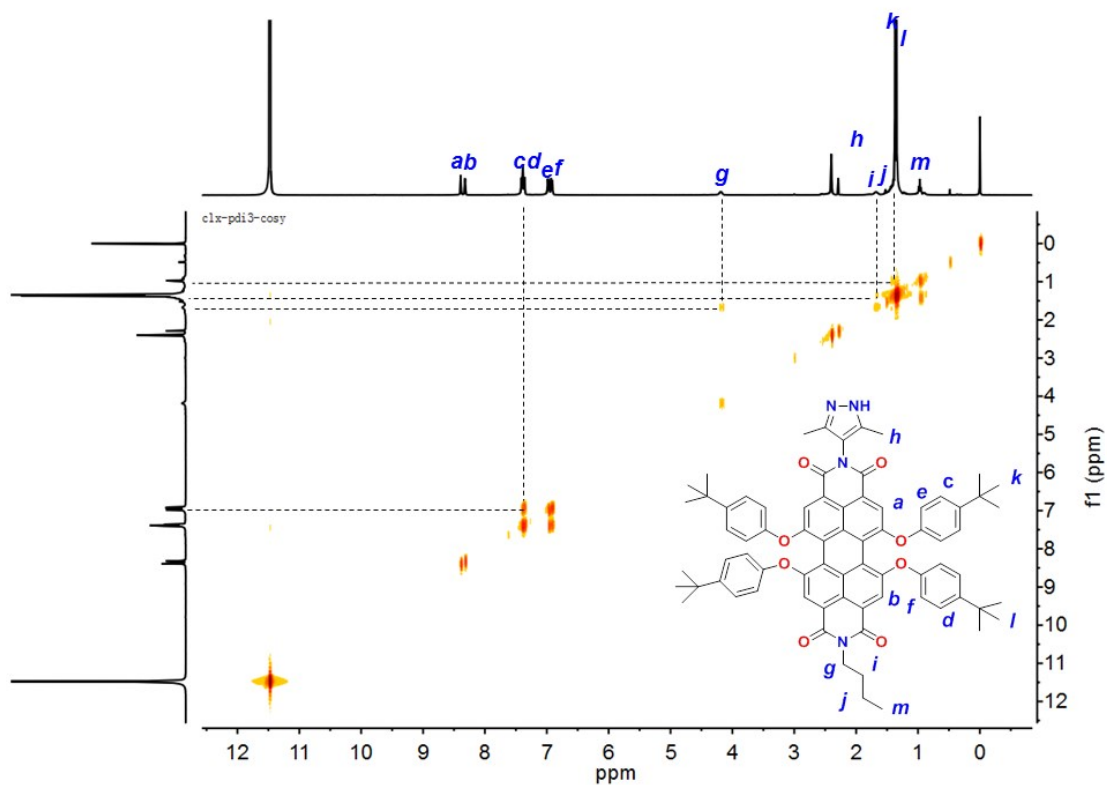


Figure S11  $^1\text{H}$ - $^1\text{H}$  COSY spectrum of ligand **3** (400 MHz,  $\text{CF}_3\text{COOD}$ , 298 K).

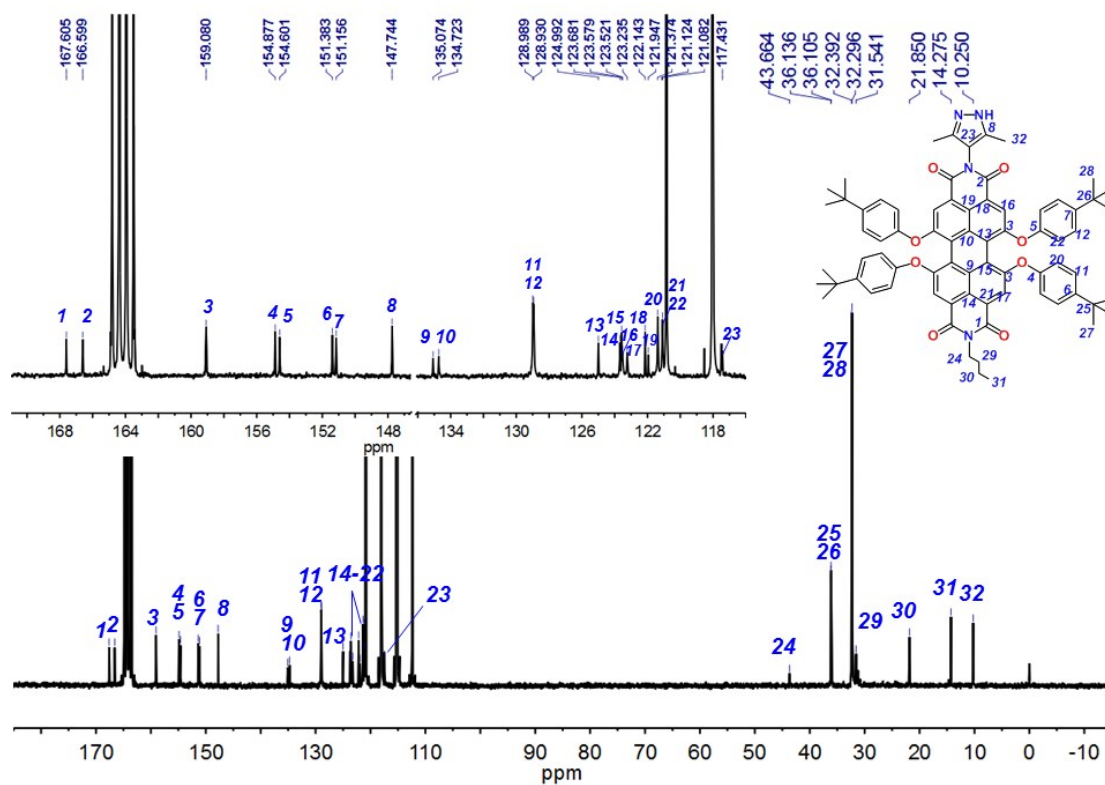


Figure S12  $^{13}\text{C}$  NMR spectrum of ligand **3** (100 MHz,  $\text{CF}_3\text{COOD}$ , 298 K).

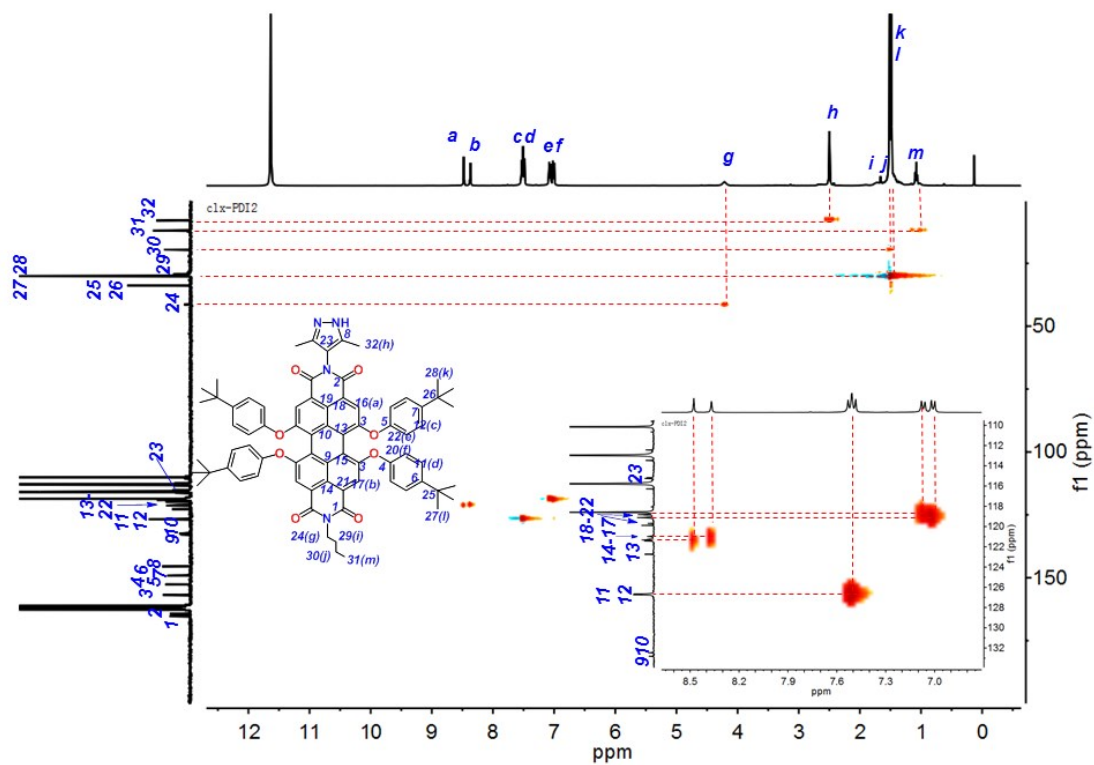


Figure S13  $^1\text{H}$ - $^{13}\text{C}$  HSQC spectrum of ligand **3** (400 MHz,  $\text{CF}_3\text{COOD}$ , 298 K).

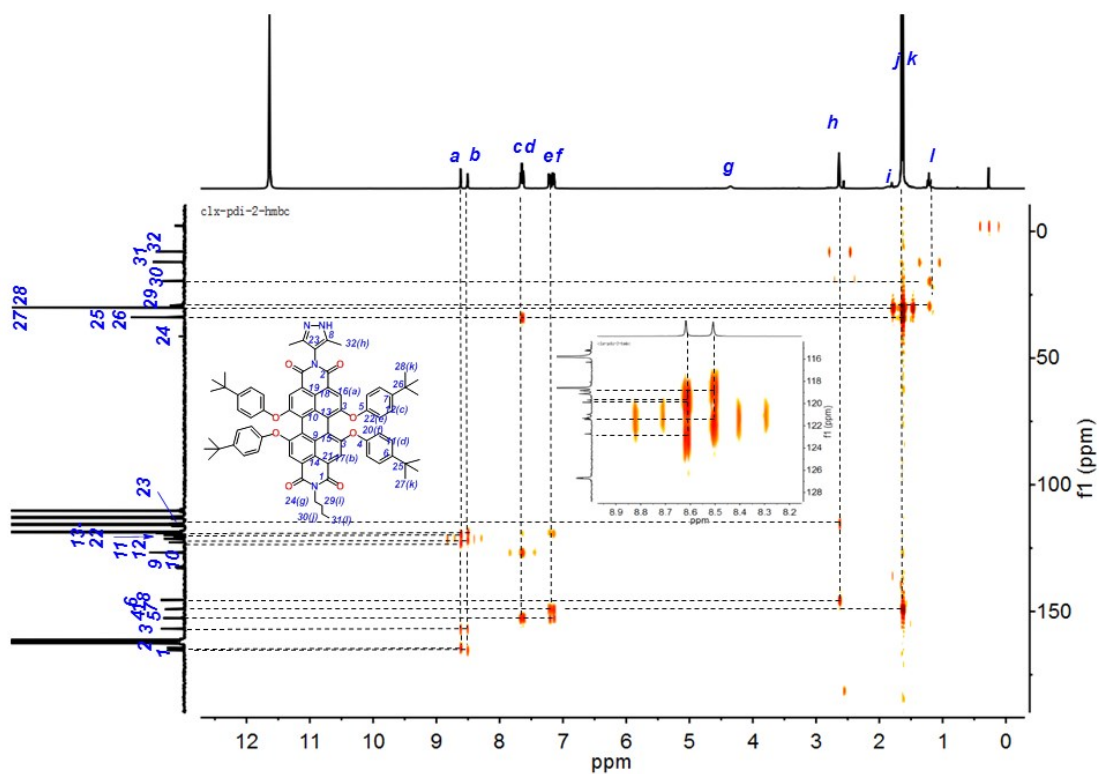
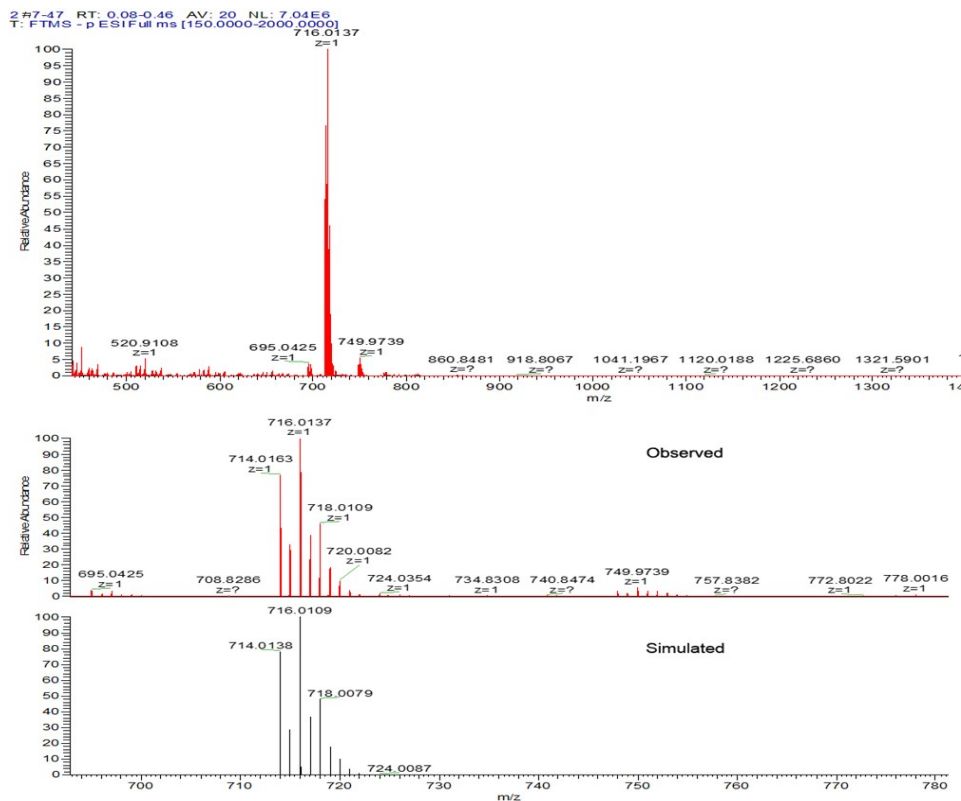
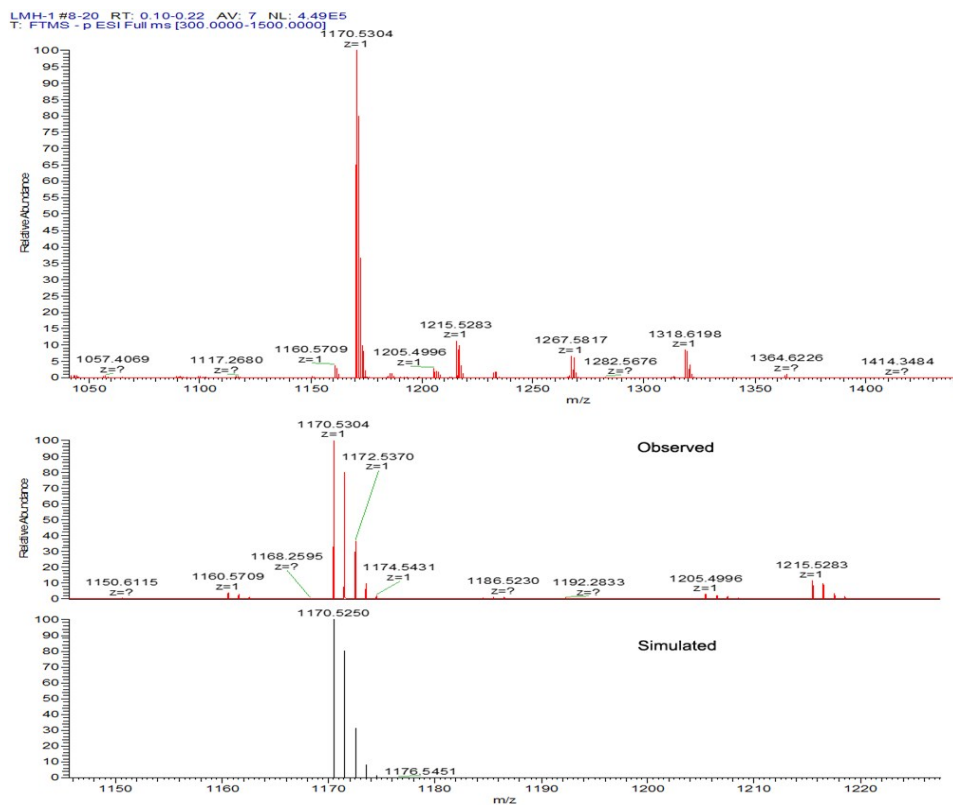


Figure S14  $^1\text{H}$ - $^{13}\text{C}$  HMBC spectrum of ligand **3** (400 MHz,  $\text{CF}_3\text{COOD}$ , 298 K).



**Figure S15** ESI-MS (negative mode) of **S1** with the observed and simulated isotope patterns of the  $[M-H]^-$  peak.



**Figure S16** ESI-MS (negative mode) of ligand **1** with the observed and simulated isotope patterns of the  $[M-H]^-$  peak.

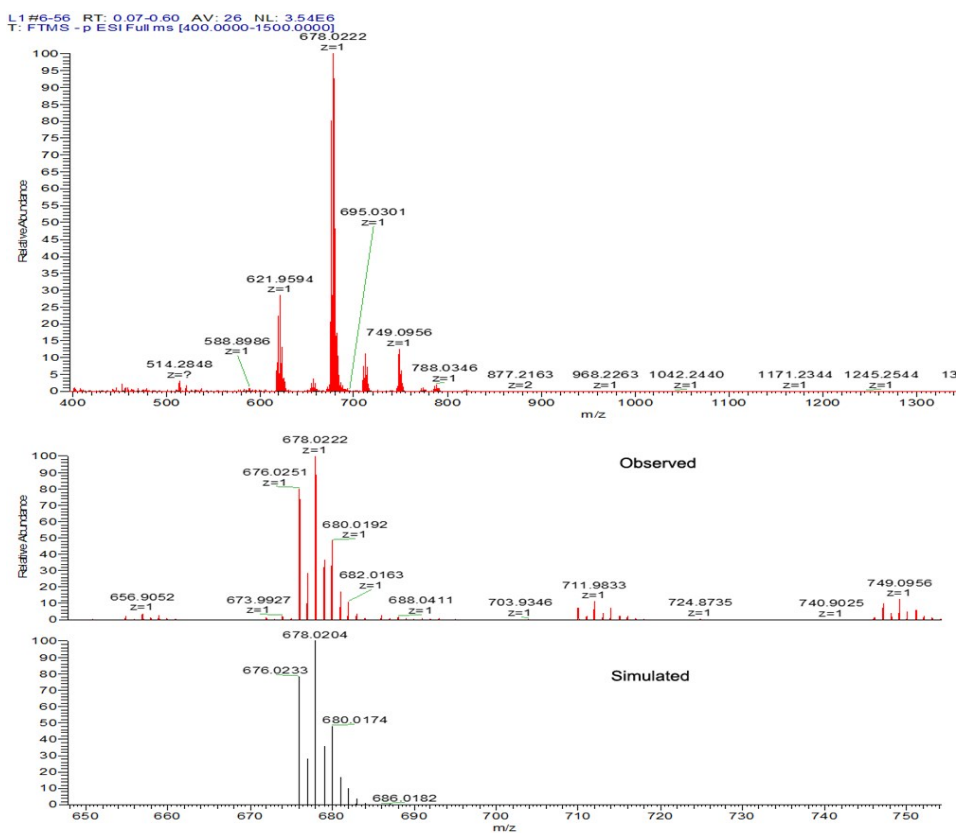


**Figure S17** ESI-MS (negative mode) of **S2** with the observed and simulated isotope patterns of the  $[M-H]^-$  peak.

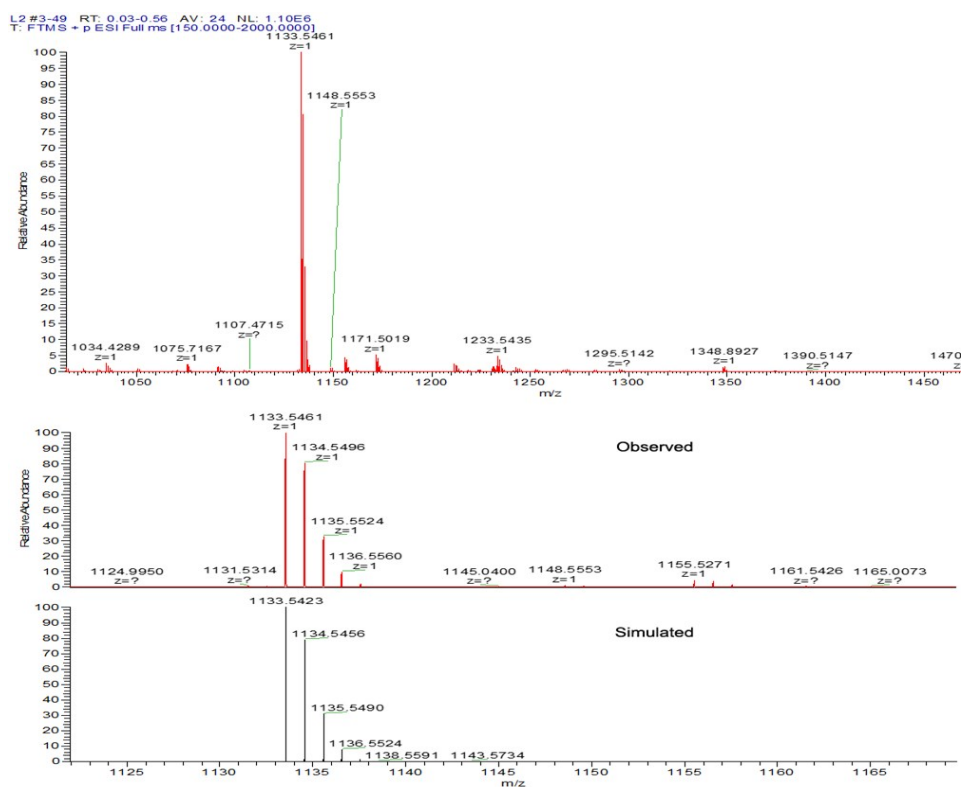


**Figure S18** ESI-TOF-MS (positive mode) of ligand **3** with the observed and simulated isotope patterns of the  $[M+H]^+$  peak.

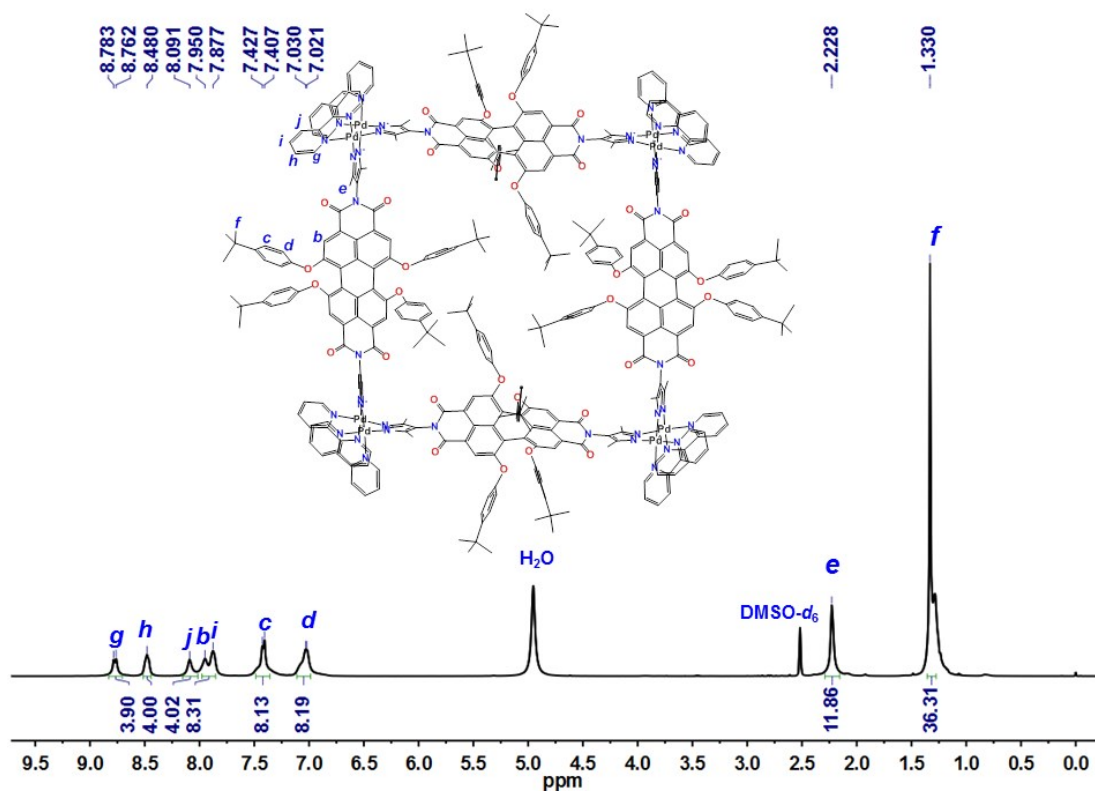


**Figure S19**  $^1\text{H}$  NMR spectra of metallacycle **2** (400 MHz, DMSO- $d_6$ , 298 K).

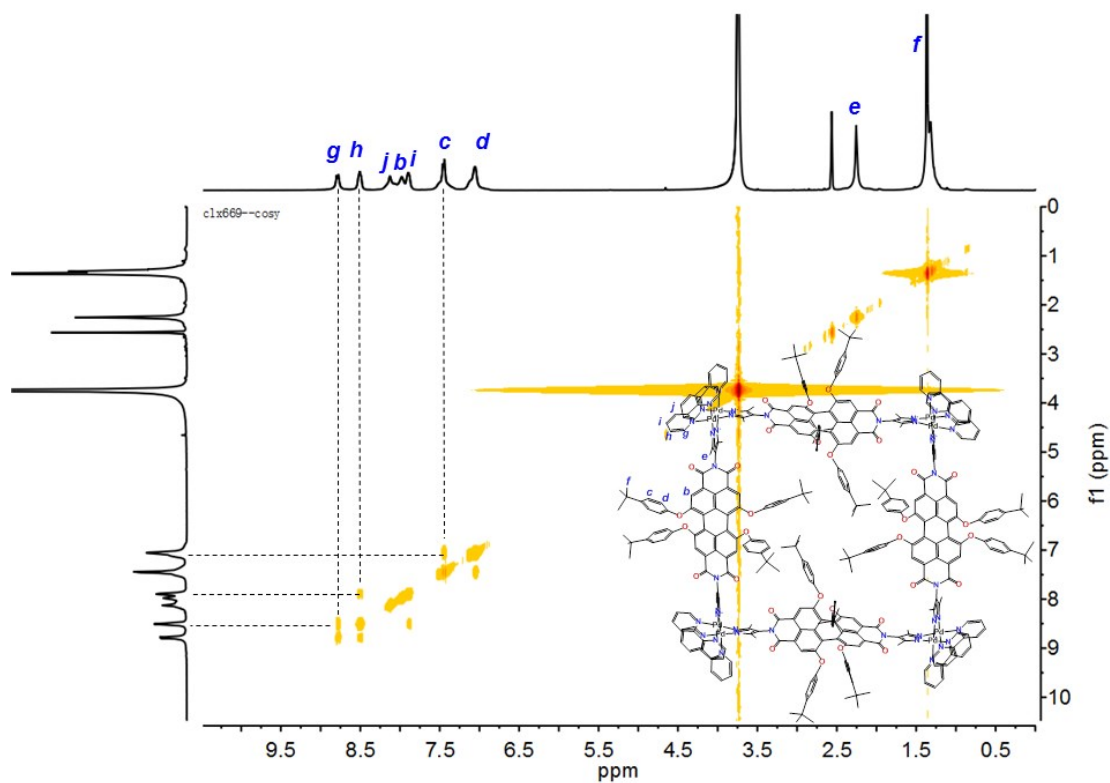


Figure S20  $^1\text{H}$ - $^1\text{H}$  COSY spectrum of metallacycle **2** (400 MHz,  $\text{DMSO-}d_6$ , 298 K).

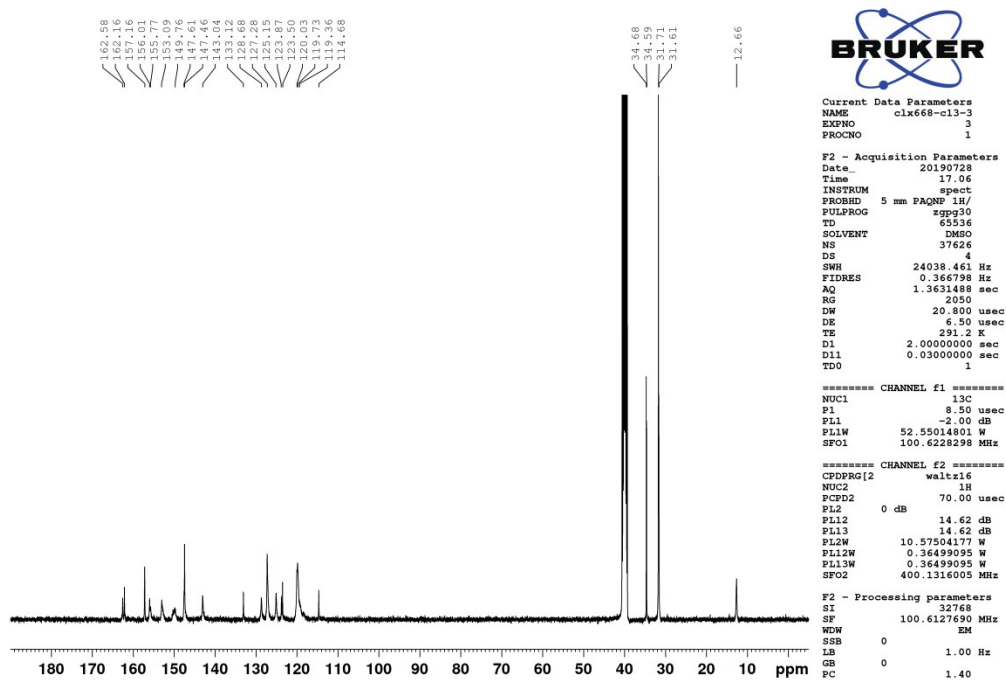


Figure S21  $^{13}\text{C}$  NMR spectrum of metallacycle **2** (100 MHz,  $\text{DMSO-}d_6$ , 298 K). The  $^{13}\text{C}$  NMR for

this compound is difficult to measure possibly due to aggregation and poor solubility.

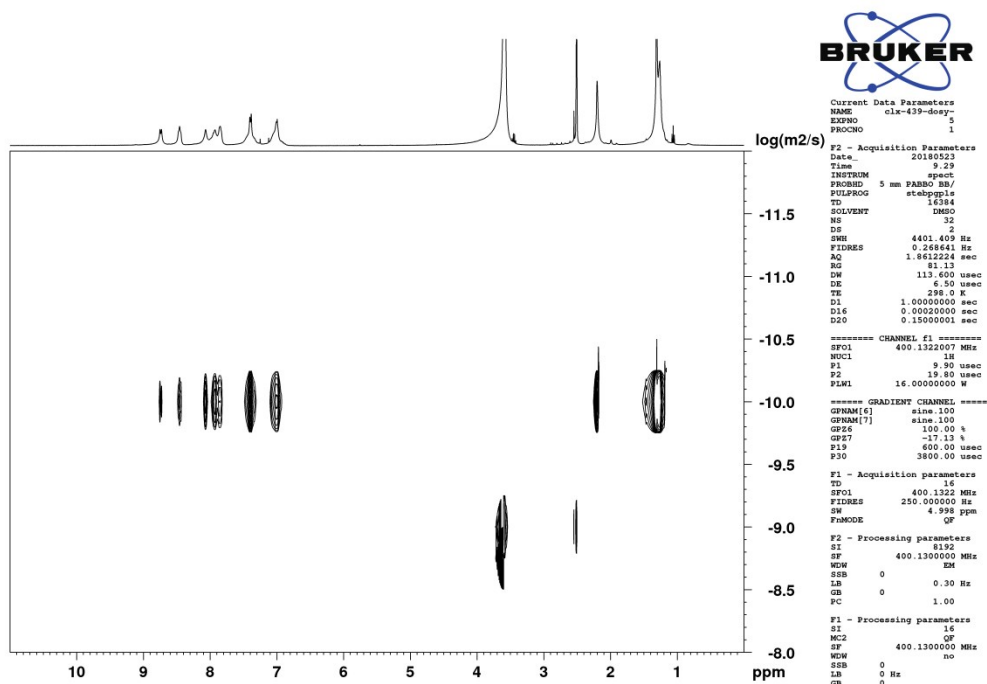


Figure S22  $^1\text{H}$  DOSY spectrum of metallacycle 2 (400 MHz,  $\text{DMSO-}d_6$ , 298 K).

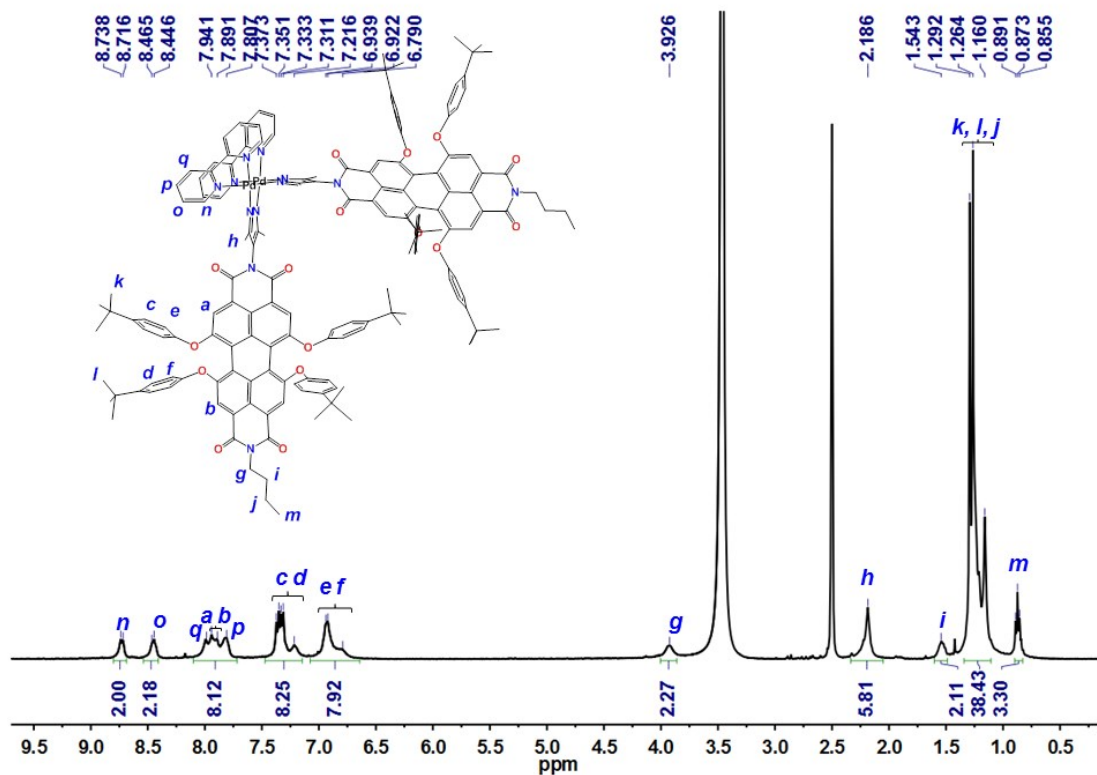


Figure S23  $^1\text{H}$  NMR spectrum of complex 4 (400 MHz,  $\text{DMSO-}d_6$ , 298 K).

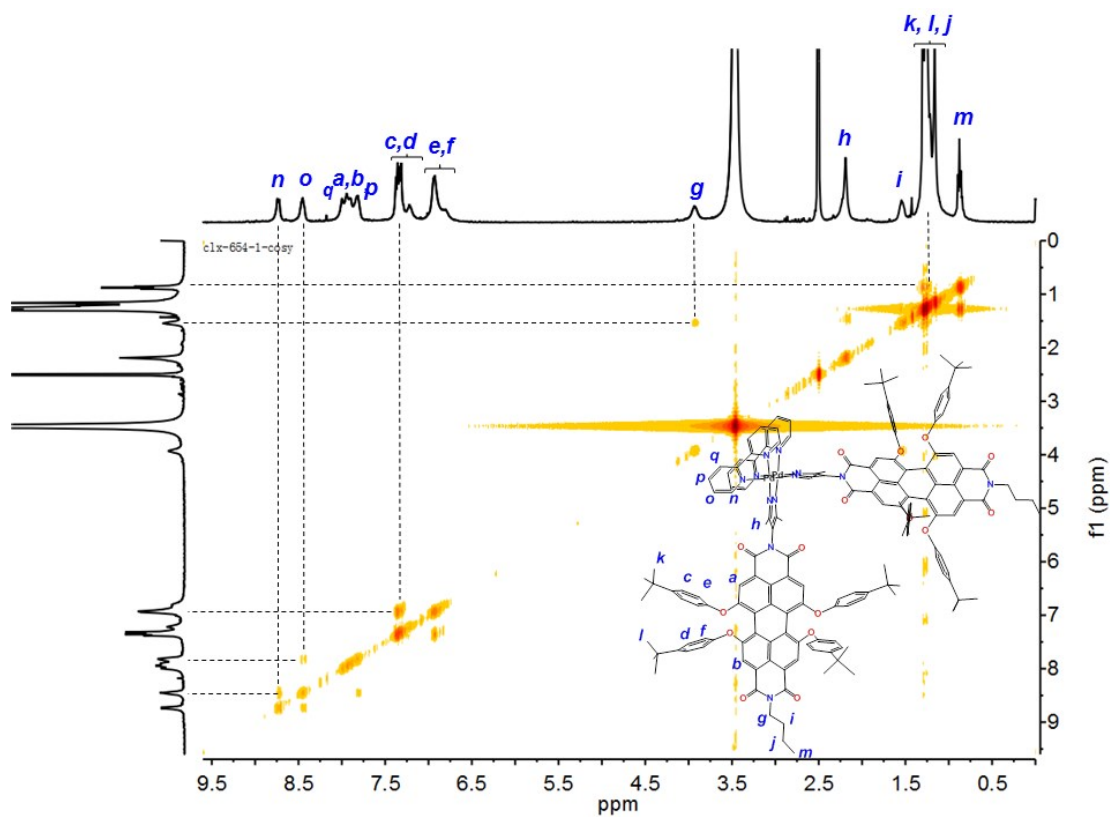
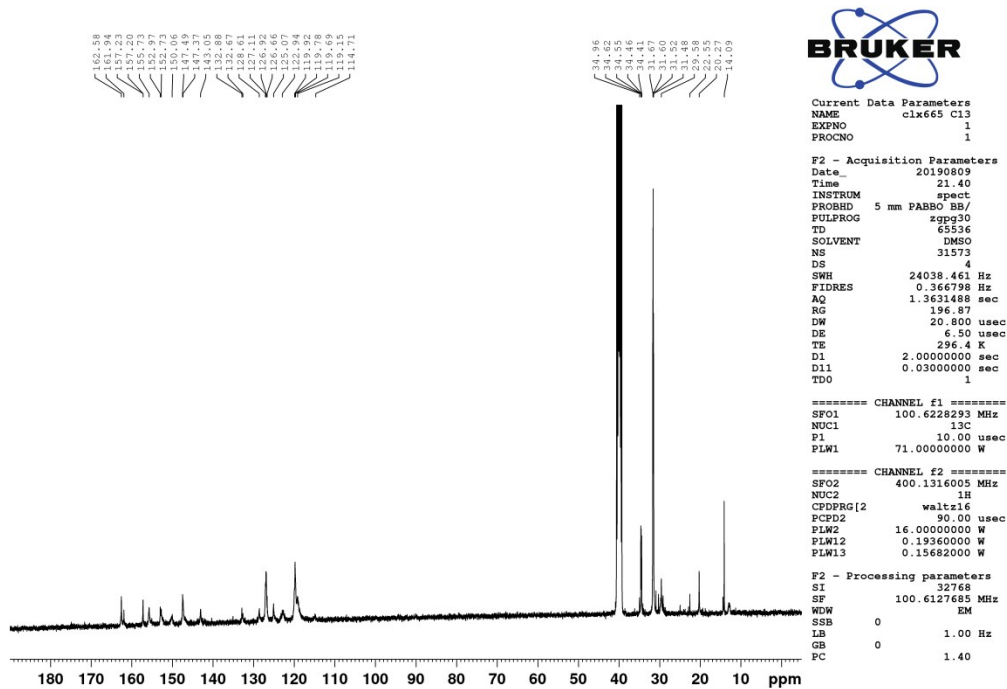
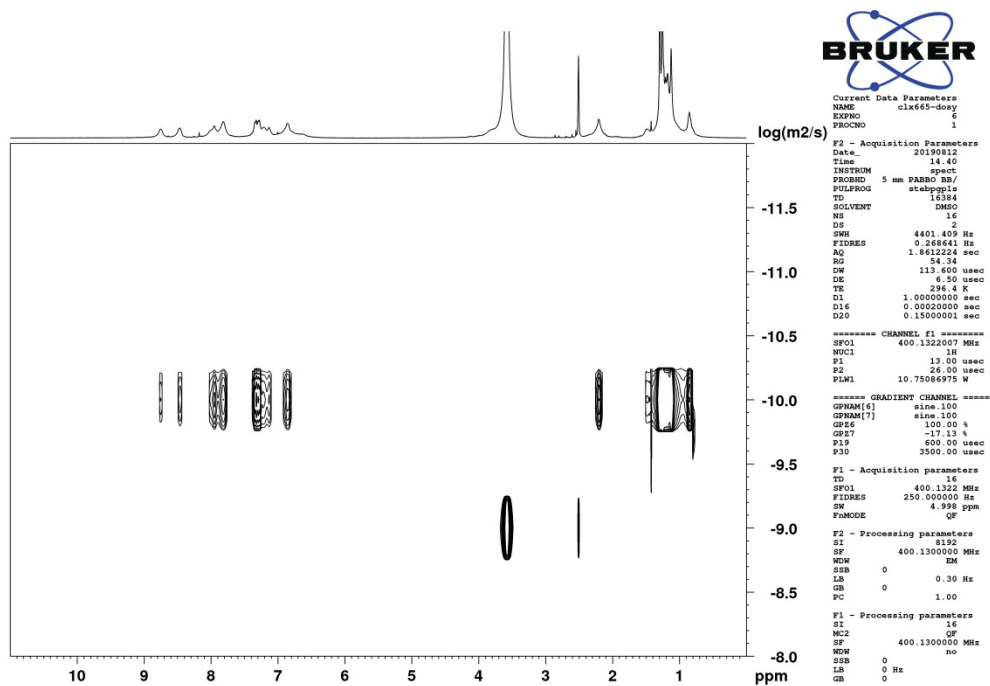


Figure S24  $^1\text{H-}^1\text{H}$  COSY spectrum of complex 4 (400 MHz,  $\text{DMSO-}d_6$ , 298 K).



**Figure S25**  $^{13}\text{C}$  NMR spectrum of complex **4** (400 MHz,  $\text{DMSO-}d_6$ , 298 K). The  $^{13}\text{C}$  NMR for this compound is difficult to measure possibly due to aggregation and poor solubility.



**Figure S26**  $^1\text{H}$  DOSY spectrum of complex **4** (400 MHz,  $\text{DMSO-}d_6$ , 298 K).

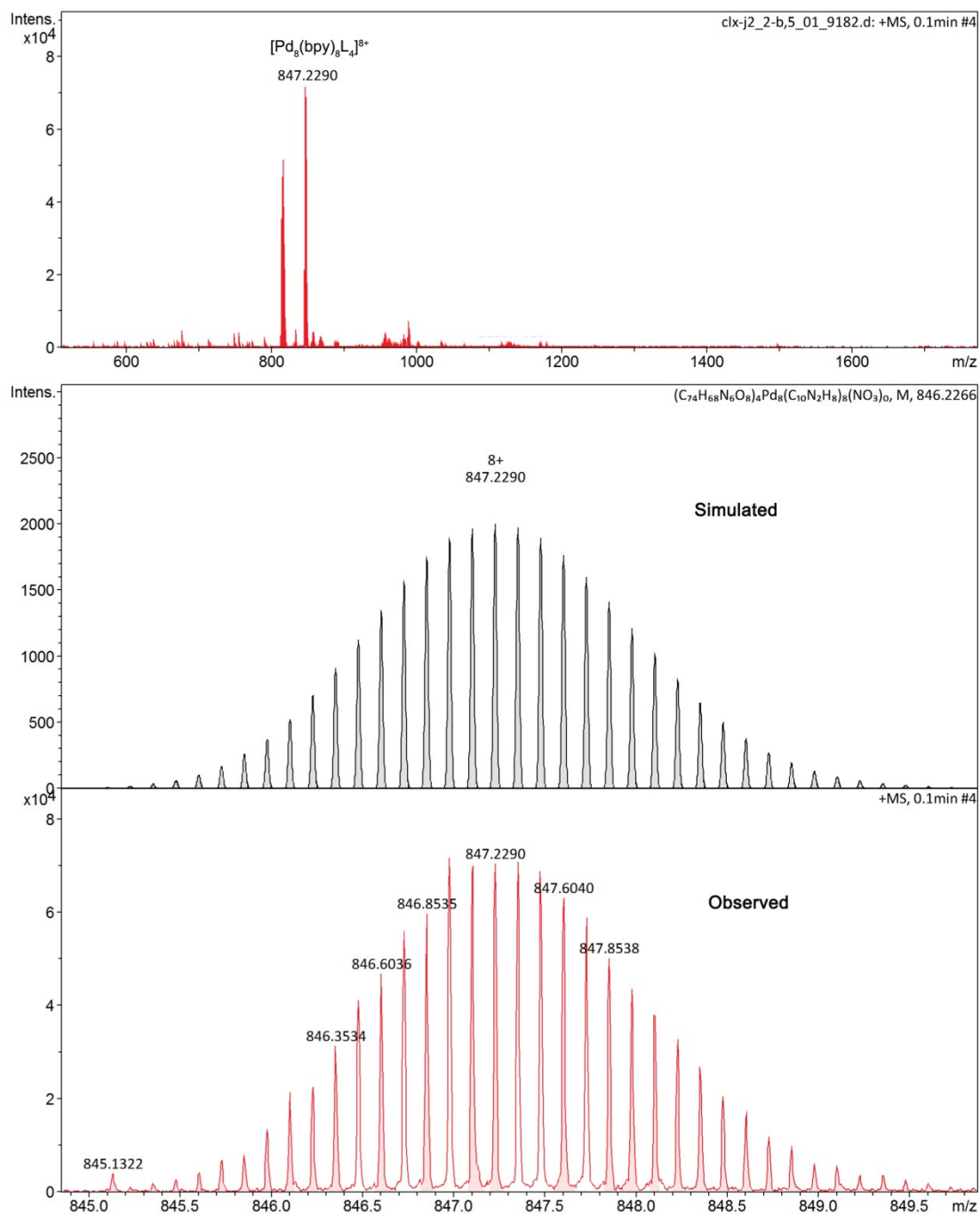


**Figure S27** ESI-TOF-MS (positive mode) of metallacycle **2** with the observed and simulated isotope patterns of the  $[\text{M}-8\cdot\text{NO}_3]^{8+}$  peak.

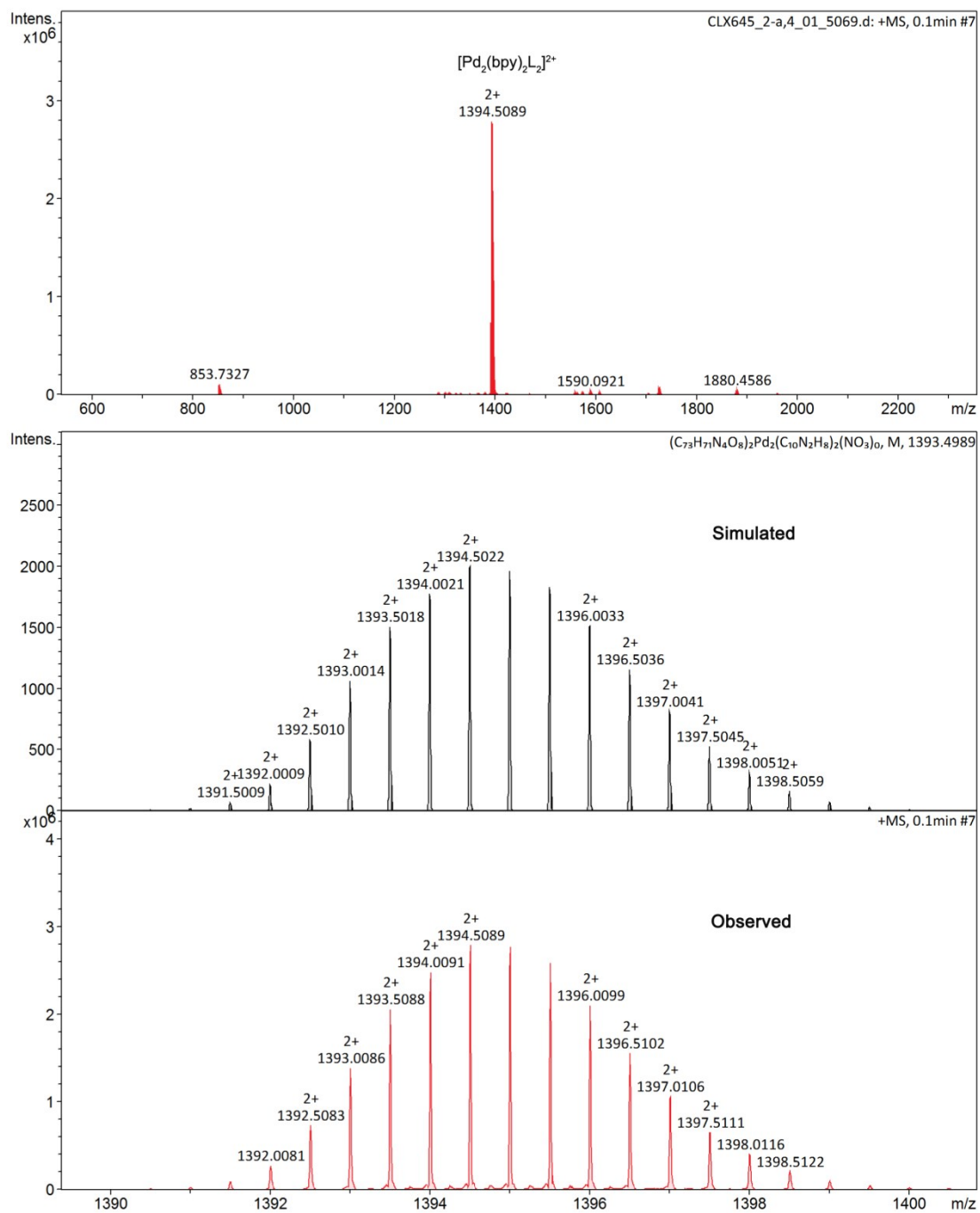


**Figure S28** ESI-TOF-MS (positive mode) of complex **4** with the observed and simulated isotope patterns of the  $[M-2\cdot\text{NO}_3]^{2+}$  peak.

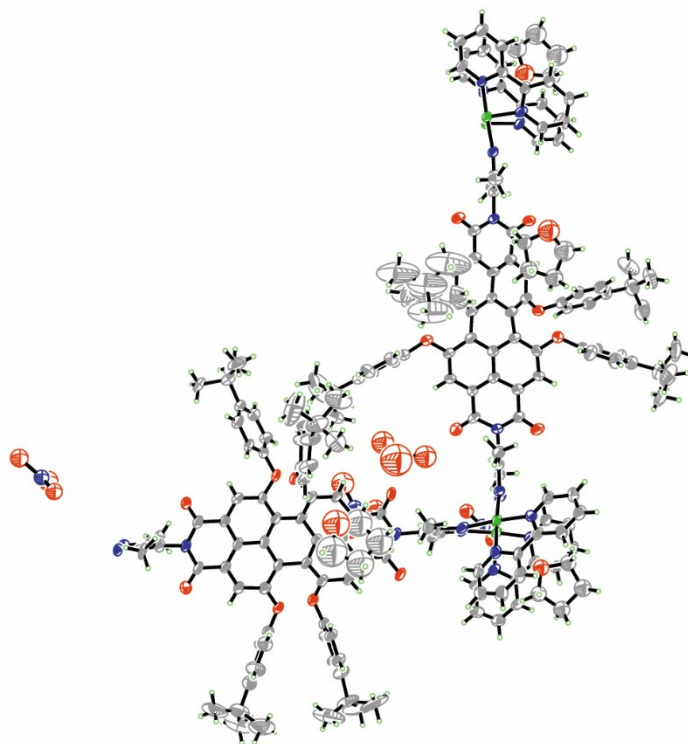


**Figure S29** Ortep drawing of the asymmetric unit in the crystal structure of metallacycle **2** at 30% probability level. C gray, H white, N blue, O red, Pd green.

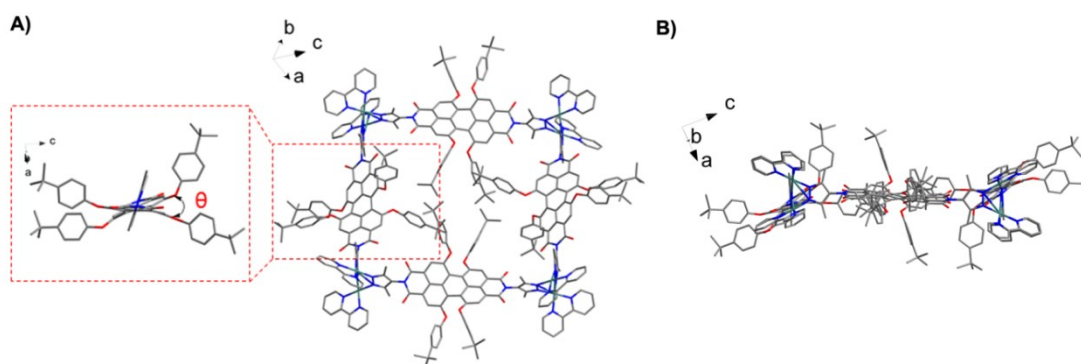


**Figure S30** (A) The preferred conformation of the phenoxy substituents of bay-substituted Perylene-Diimide ligands in the structure of **2**, showing a propeller-like conformation with the dihedral angles of the two naphthalene subunits. (B) Side view for the structure of metallacycle **2**.

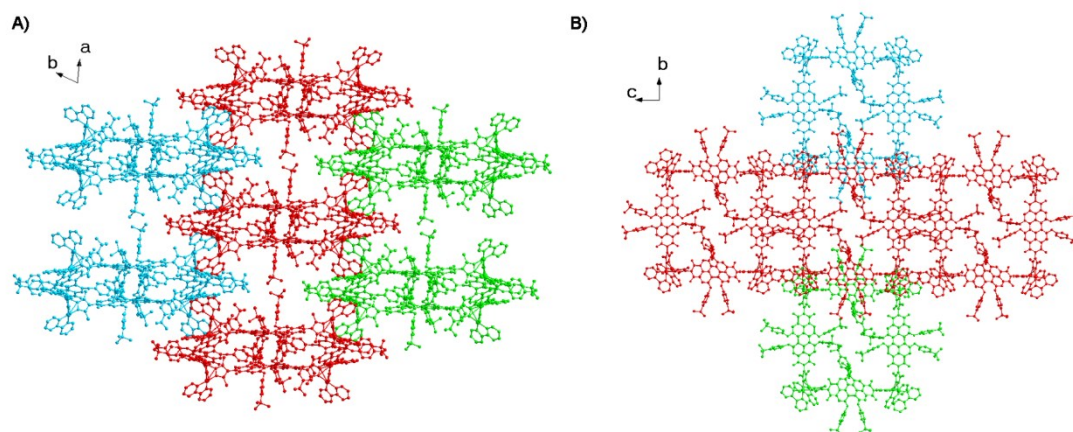


**Figure S31** Crystal structure packing of metallacycle **2** from the view along (A) c axis and (B) a axis. The solvents, counter ions and all H atoms are omitted for clarity. The steric congestion evoked by *t*-butylphenol substituents in the bay positions leads to the core distortion and suppresses the aggregation of the central perylene diimide chromophores toward face-to-face  $\pi$ - $\pi$  stacking.

## Section C. Photophysical properties and singlet oxygen production

### 1. Photophysical data for all compounds 1-4.

The absolute quantum yield (QY) measurement was performed on the FS5 spectrofluorometer from Edinburg Photonics (SC-30 Intergrating Sphere). The QY is defined as:

$$\text{QY} = \frac{\text{number of photon emitted}}{\text{number of photon absorbed}} = \frac{L_{\text{sample}}}{E_{\text{reference}} - E_{\text{sample}}}$$

where QY is the quantum yield,  $L_{\text{sample}}$  is the emission intensity of sample,  $E_{\text{reference}}$  and  $E_{\text{sample}}$  are the intensities of the excitation light not absorbed by the sample and the reference sample, respectively.<sup>S6</sup> For our liquid samples, the reference would be a cuvette containing DMSO only.

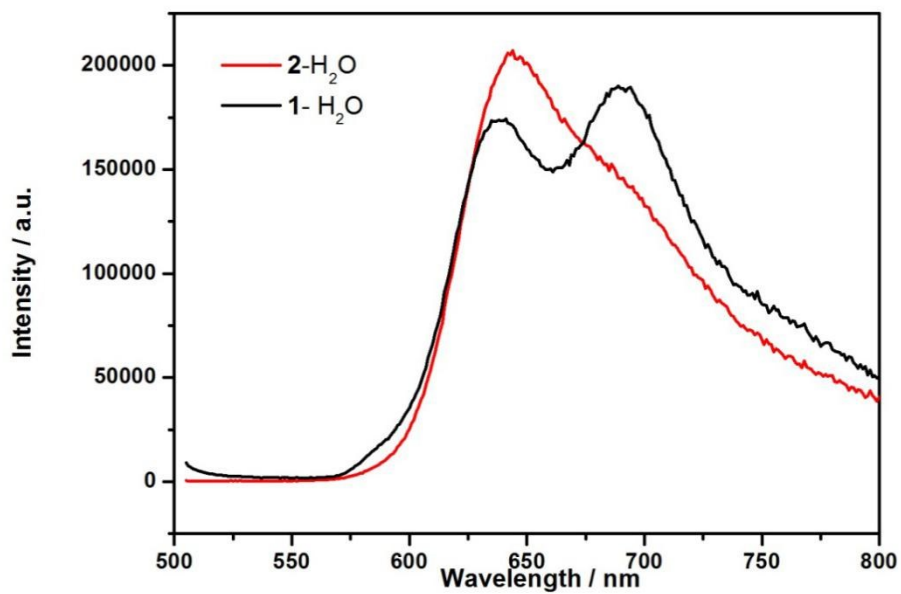


**Figure S32** The emission spectra of ligand **1** (black) and metallacycle **2** (red) in H<sub>2</sub>O (c = 10 μM, slits = 6-4).

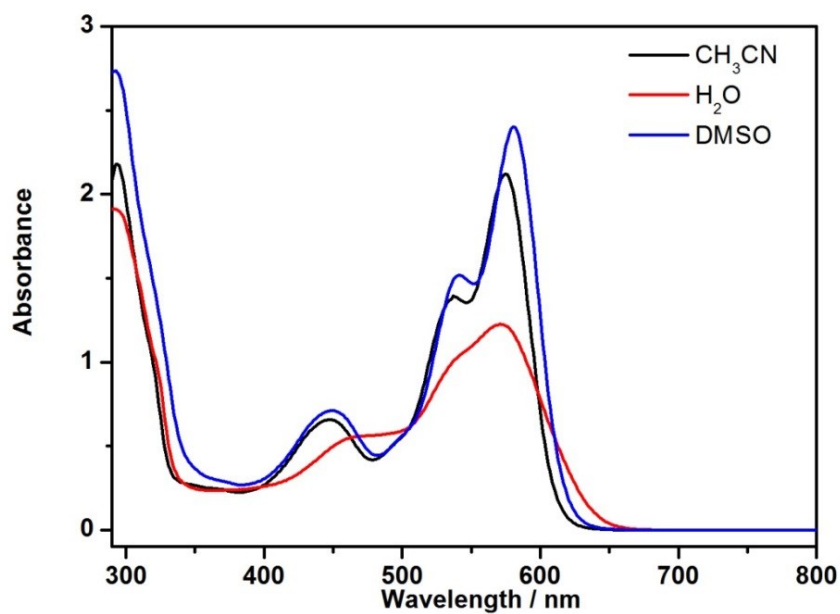


**Figure S33** The UV-Vis spectra of metallacycle **2** in different solvents.

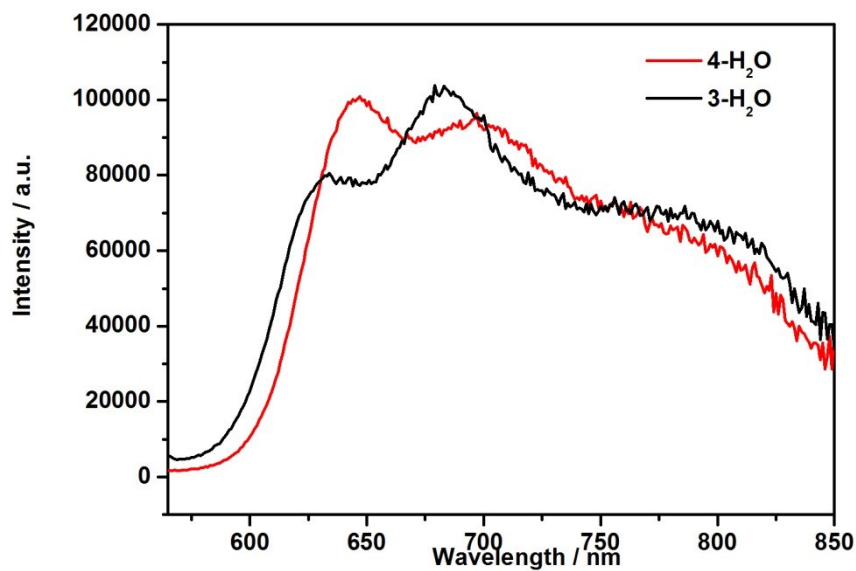


**Figure S34** The emission spectra of ligand **3** and complex **4** in H<sub>2</sub>O ( $c = 10 \mu\text{M}$ , slits = 6-4).

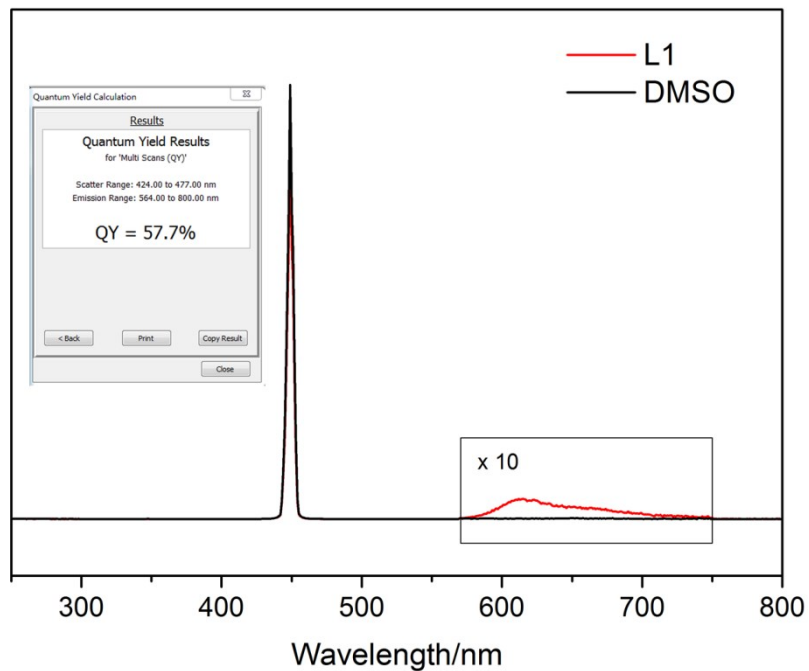


**Figure S35** Quantum yield of ligand **1** in DMSO (298 K,  $c = 2 \times 10^{-6} \text{ M}$ ,  $\lambda_{\text{ex}} = 447 \text{ nm}$ , QY = 57.7%).

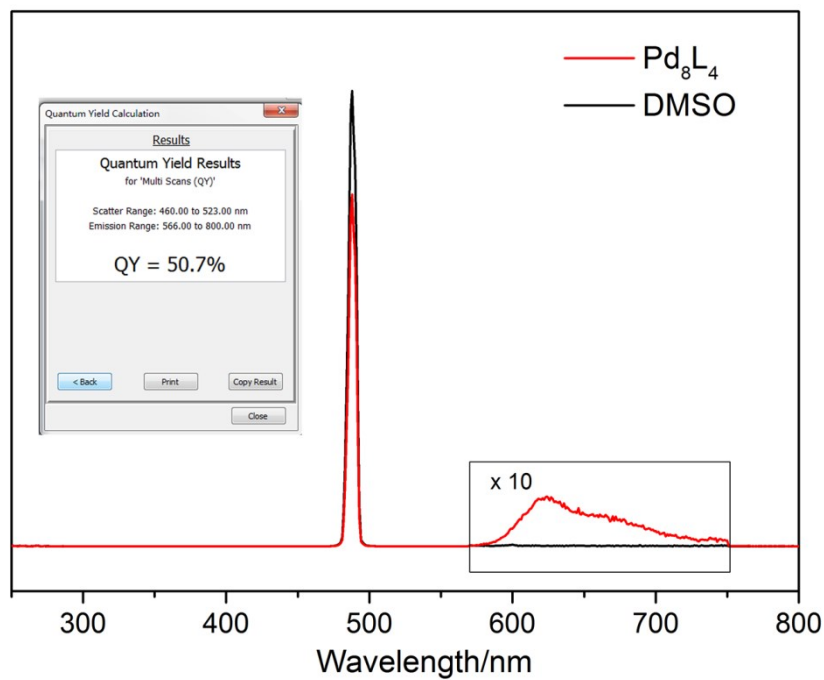


**Figure S36** Quantum yield of metallacycle **2** in DMSO (298 K,  $c = 2 \times 10^{-6}$  M,  $\lambda_{\text{ex}} = 486$  nm, QY = 50.7%).

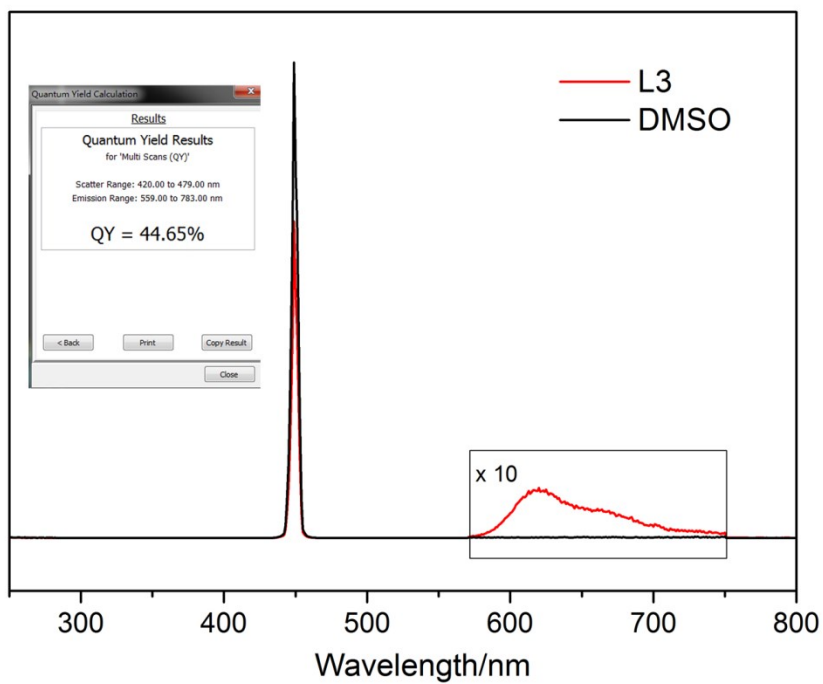


**Figure S37** Quantum yield of ligand **3** in DMSO (298 K,  $c = 8 \times 10^{-6}$  M,  $\lambda_{\text{ex}} = 447$  nm, QY = 44.7%).

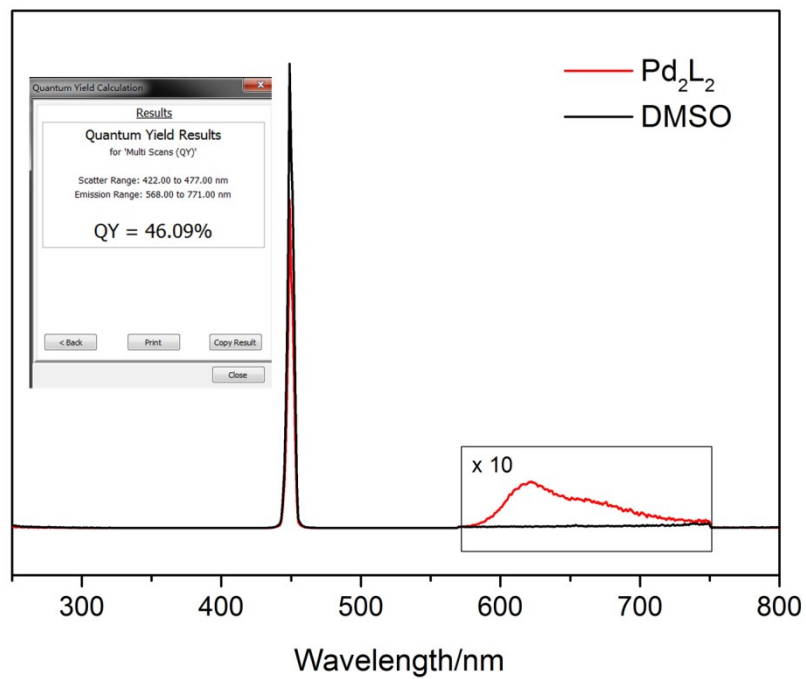


**Figure S38** Quantum yield of complex **4** in DMSO (298 K,  $c = 4 \times 10^{-6}$  M,  $\lambda_{\text{ex}} = 447$  nm, QY = 46.1%).

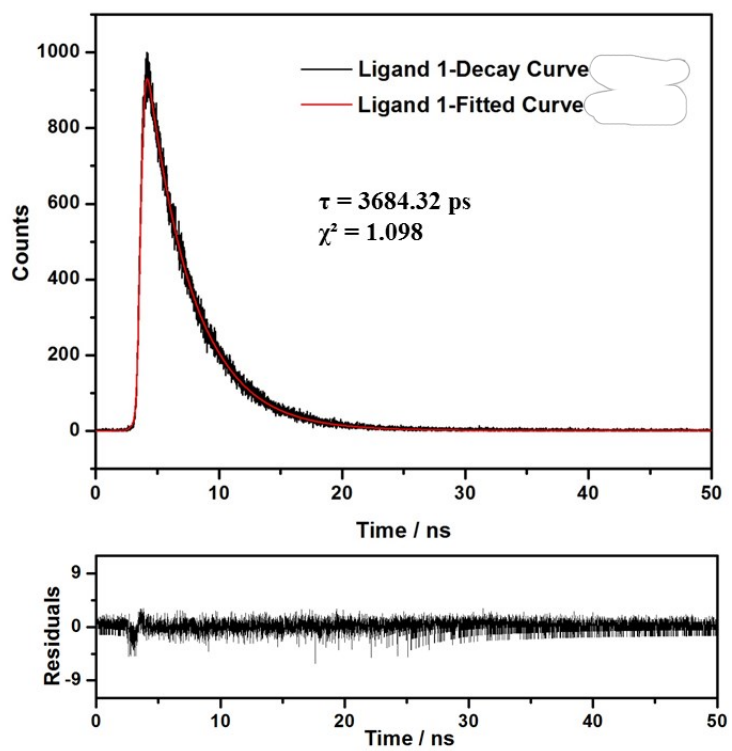


**Figure S39** Excited state decay curve with single exponential fit for ligand **1** under anaerobic condition at 298 K ( $\lambda_{\text{ex}} = 377$  nm).

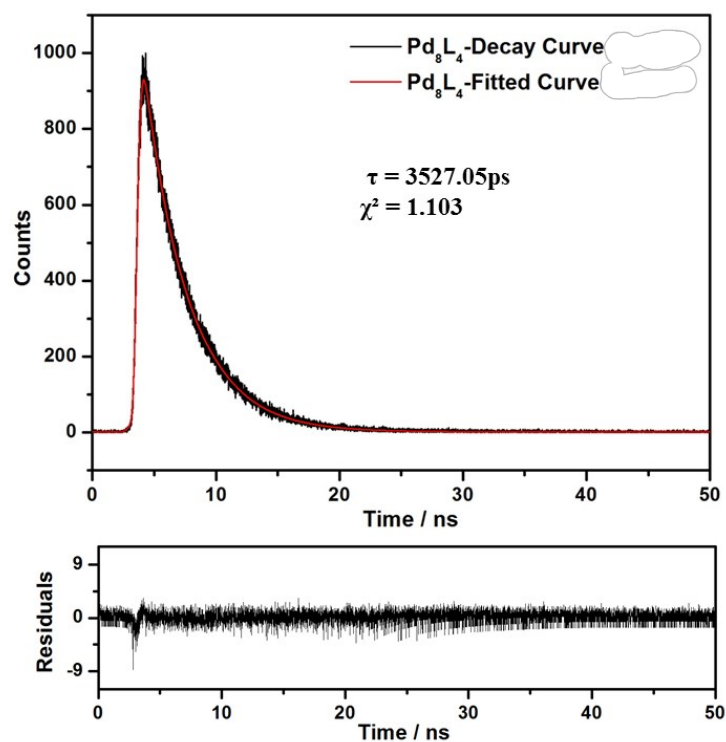


**Figure S40** Excited state decay curve with single exponential fit for metallacycle **2** under anaerobic condition at 298 K ( $\lambda_{\text{ex}} = 377$  nm).

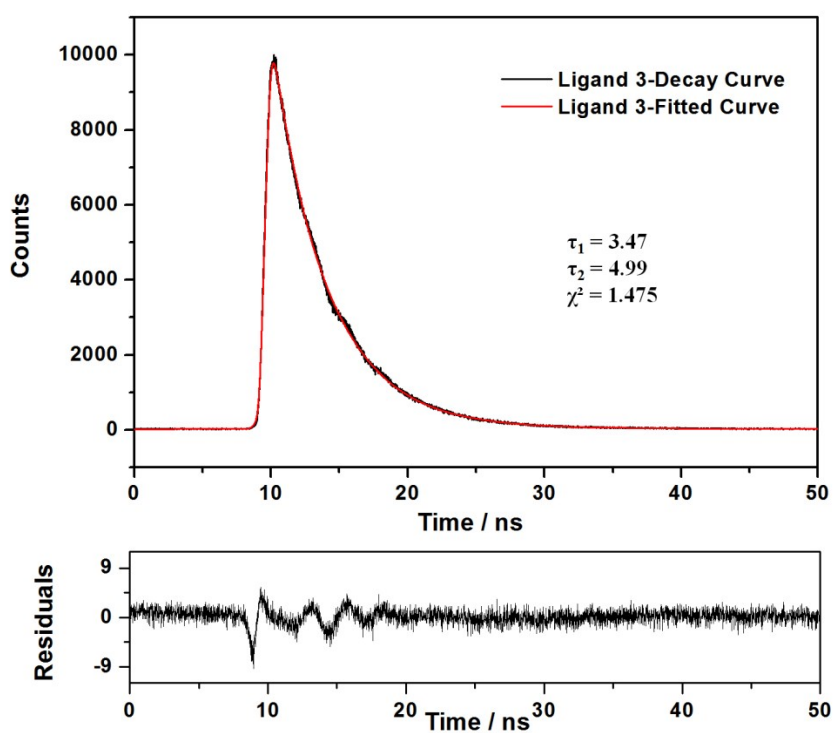


**Figure S41** Excited state decay curve with single exponential fit for ligand **3** under anaerobic

conditions at 298 K ( $\lambda_{\text{ex}} = 377$  nm).

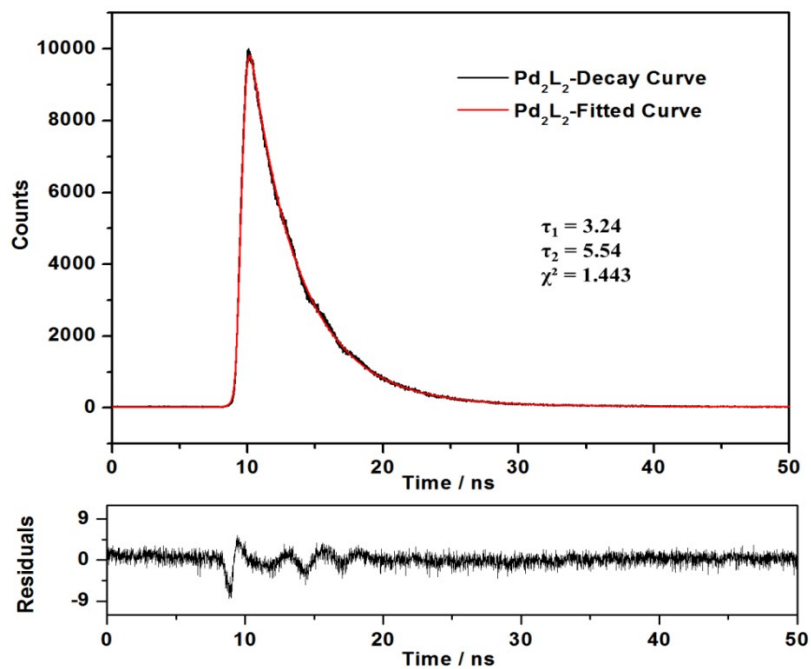


**Figure S42** Excited state decay curve with single exponential fit for complex **4** under anaerobic condition at 298 K ( $\lambda_{\text{ex}} = 377$  nm).

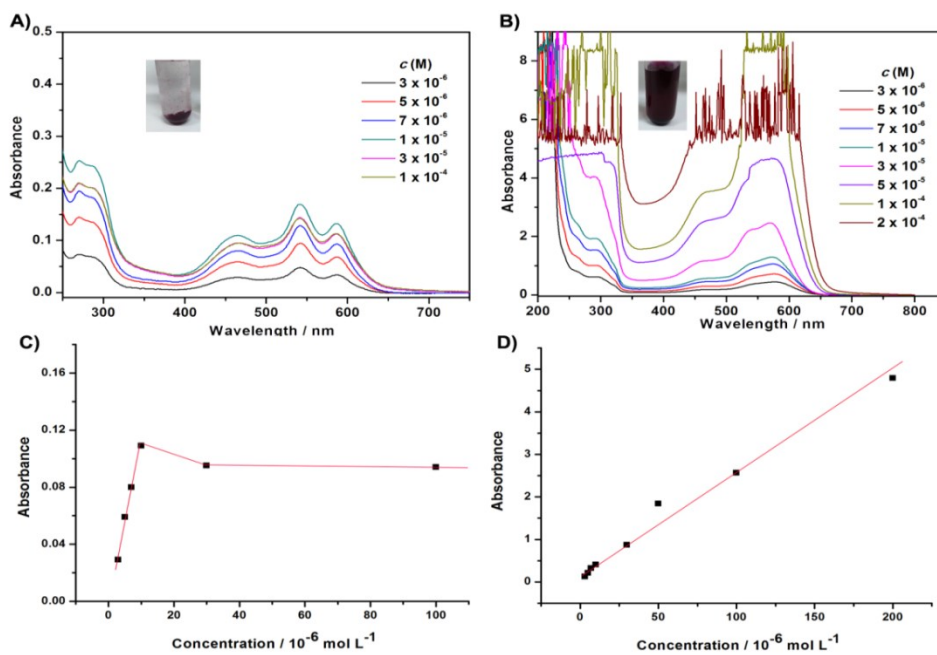


**Figure S43** The concentration-dependent UV-Vis absorption spectra of ligand **1** (A) and metallacycle **2** (B) in solution ( $V_{\text{water}}/V_{\text{DMSO}} = 150/1$ ), which revealed that the absorbance of ligand **1** starts to level-off when its concentration is beyond  $3 \times 10^{-5}$  M, while that of the metallacycle **2** keeps increasing up to  $3 \times 10^{-4}$  M. This indicates that the cationic metallacycle **2** has much better water solubility than free ligand **1**. Inserted photos show the solubility of ligand **1** and metallacycle **2** at the concentration of  $1 \times 10^{-5}$  M. The plots of absorbance at 463 nm for ligand **1** (C) and 436 nm for metallacycle **2** (D) versus concentration.

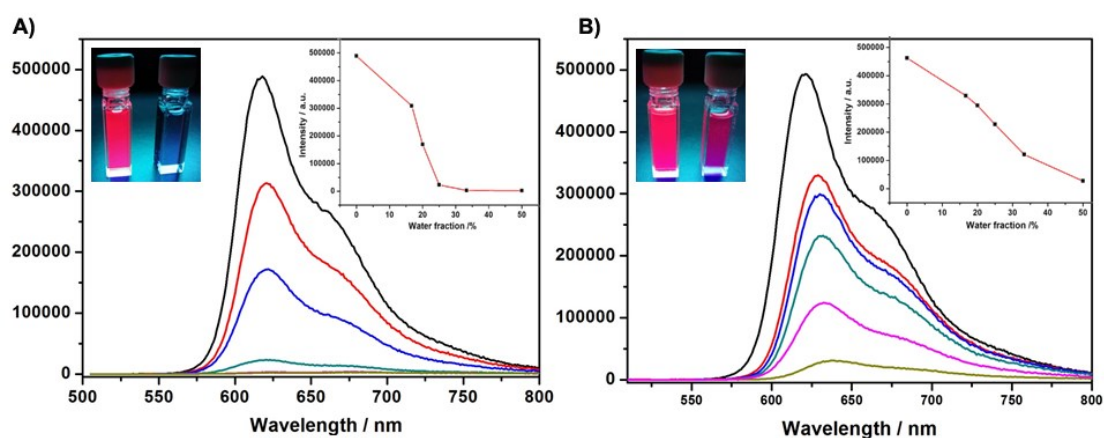


**Figure S44** Fluorescence emission spectra of (A) Ligand **1** and (B) metallacycle **2** ( $\lambda_{\text{ex}} = 486$  nm,  $c_{\text{Pd8L4}} = 6.25 \mu\text{M}$ ,  $c_{\text{L}} = 25.00 \mu\text{M}$ , slits = 1.5-1) with insets showing the plots of maximum emission intensity of ligands versus  $\text{H}_2\text{O}$  fraction in  $\text{H}_2\text{O}/\text{DMSO}$  mixtures and photographs of corresponding compound in pure DMSO and 50 %  $\text{H}_2\text{O}$  fractions mixed solution upon excitation at 365 nm using an UV lamp.

**Table S2.** Summary of photophysical data.

Cpd	$\lambda_{\text{max}}^{\text{abs}}$ (nm)		$\epsilon / 10^5 (\text{M}^{-1}\text{cm}^{-1})$		$\lambda_{\text{max}}^{\text{em}}$ (nm)		$\tau_{\text{obs}}$ (ns)	QY (%)
	DMSO	Water	DMSO	Water	DMSO	Water		
<b>1</b>	578	541	0.39	0.19	617	638/686	3.684	57.7 ( $\lambda_{\text{ex}} = 447\text{nm}$ )

								51.0 ( $\lambda_{\text{ex}} = 537\text{nm}$ )
$\text{Pd}_8\text{L}_4$ <b>2</b>	580	571	1.55	1.23	627	644	3.527	50.7 ( $\lambda_{\text{ex}} = 486\text{nm}$ )
<b>3</b>	577	582	0.33	0.17	618	683/634	3.24 ( $\tau_1, 69.7\%$ ) 5.54 ( $\tau_2, 30.3\%$ )	44.7 ( $\lambda_{\text{ex}} = 447\text{nm}$ )
$\text{Pd}_2\text{L}_2$ <b>4</b>	580	594	0.79	0.36	619	646/699	3.47 ( $\tau_1, 61.7\%$ ) 4.99 ( $\tau_2, 37.3\%$ )	46.1 ( $\lambda_{\text{ex}} = 447\text{nm}$ )

## 2. $^1\text{O}_2$ generation of all compounds in DMSO solution

The rate constants ( $k$ ) of singlet oxygen ( $^1\text{O}_2$ ) production have been measured under strictly controlled experimental conditions: 1) Photo-irradiation with a Xe lamp with wavelength of 510 ( $\pm 10$ ) nm at calibrated photo-power of  $0.25 \text{ W cm}^{-2}$ ; 2) DPBF ( $150 \mu\text{M}$ ) was used as  $^1\text{O}_2$  scavenger in DMSO solvent; 3) The optical density at 510 nm ( $\text{OD}_{510 \text{ nm}}$ ) values of ligand **1** ( $c = 20 \mu\text{M}$ ), ligand **3** ( $c = 15 \mu\text{M}$ ), metallacycle **2** ( $c = 5 \mu\text{M}$ ) and complex **4** ( $c = 7.5 \mu\text{M}$ ) solutions have been adjusted to 0.25, respectively. The solutions were bubbled with  $\text{O}_2$  for 10 min before irradiation and  $\text{O}_2$  gasbag were applied to both systems. UV-visible measurements were carried out at room temperature. The  $^1\text{O}_2$  generation rate constants of the sensitizer can be calculated from  $\ln(A_0/A_t) = kt$ , where  $A_0$  and  $A_t$  denote the initial and final absorbance of DPBF at 418 nm,  $k$  is the slope of the corresponding linear curves after plotting  $\ln(A_0/A_t)$  vs time. For all compounds, the average rate constants of  $^1\text{O}_2$  generation and standard deviation are calculated from three times measurements of the  $^1\text{O}_2$  generation rate constants.

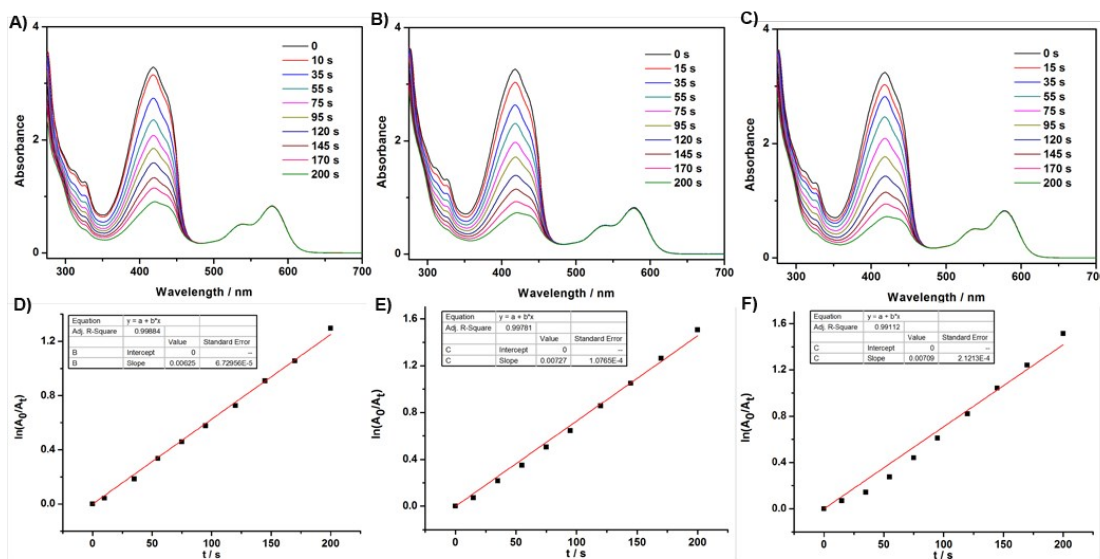


**Figure S45** (A-C) Time-dependent UV-Vis absorption spectra of DPBF in a DMSO solution of ligand **1** under O<sub>2</sub> atmosphere (Irradiation at  $\lambda_{irr} = 510$  nm). (D-E) The corresponding  $\ln(A_0/A_t)$  plots for the absorption at  $\lambda_{abs} = 418$  nm versus time. The rate constants of <sup>1</sup>O<sub>2</sub> generation for **1** were determined to be 0.0069 ( $\pm 0.0005$ ) s<sup>-1</sup>.

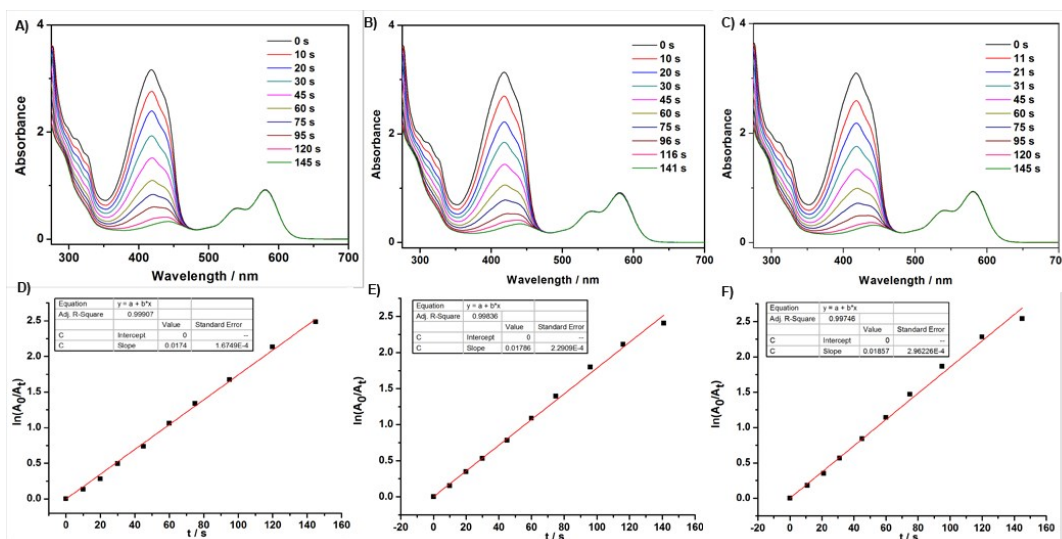


**Figure S46** (A-C) Time-dependent UV-Vis absorption spectra of DPBF in a DMSO solution of metallacycle **2** under O<sub>2</sub> atmosphere (Irradiation at  $\lambda_{irr} = 510$  nm). (D-E) The corresponding  $\ln(A_0/A_t)$  plots for the absorption at  $\lambda_{abs} = 418$  nm versus time. The rate constants of <sup>1</sup>O<sub>2</sub> generation for **2** were determined to be 0.0179 ( $\pm 0.0006$ ) s<sup>-1</sup>.

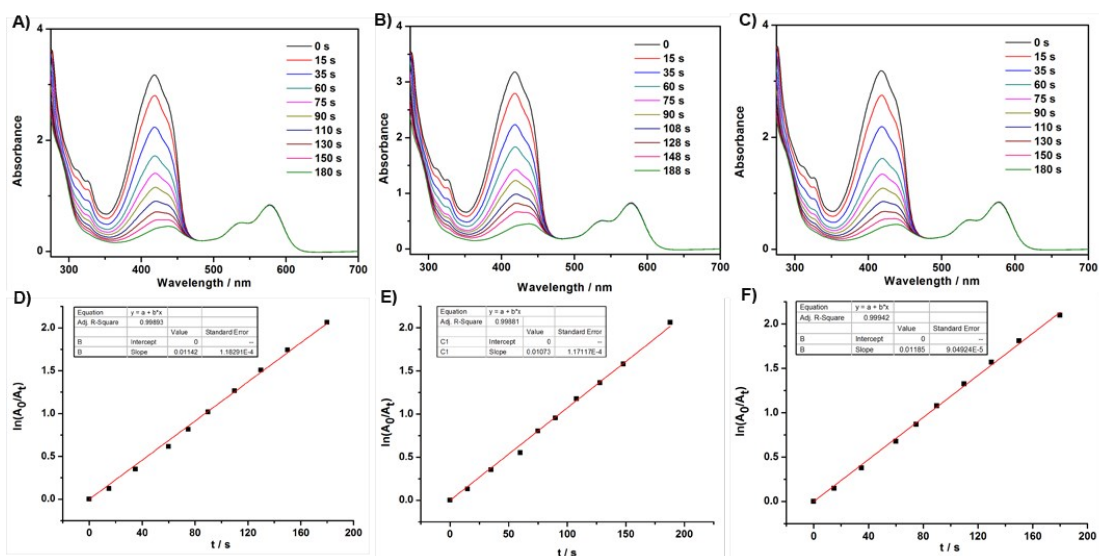


**Figure S47** (A-C) Time-dependent UV-Vis absorption spectra of DPBF in a DMSO solution of ligand **3** under O<sub>2</sub> atmosphere (Irradiation at  $\lambda_{irr} = 510$  nm). (D-E) The corresponding  $\ln(A_0/A_t)$  plots for the absorption at  $\lambda_{abs} = 418$  nm versus time. The rate constants of <sup>1</sup>O<sub>2</sub> generation for **3** were determined to be 0.0113 ( $\pm 0.0006$ ) s<sup>-1</sup>.

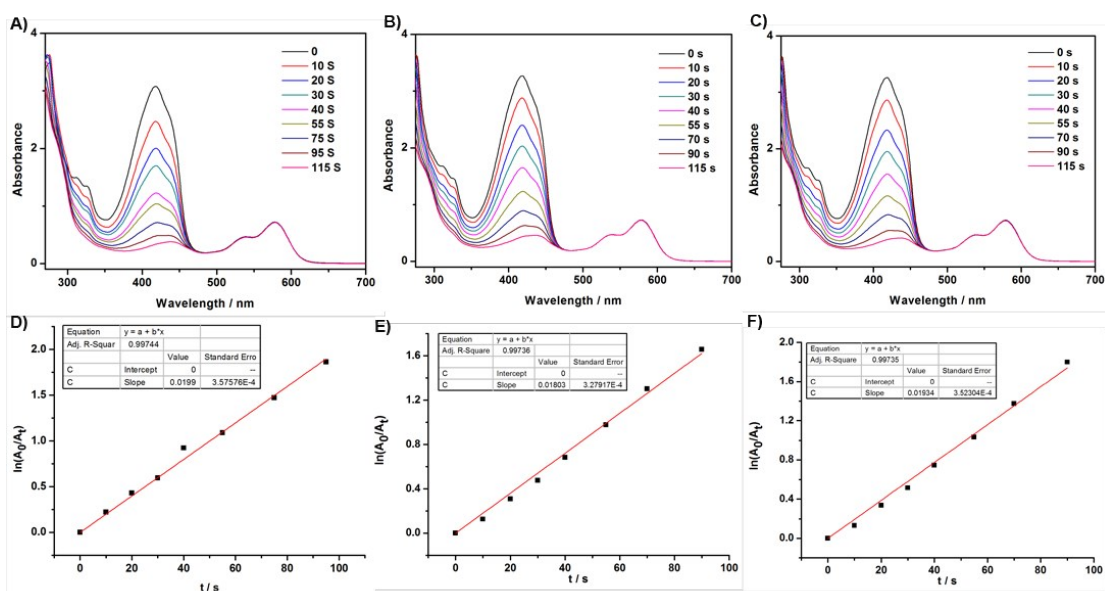


**Figure S48** (A-C) Time-dependent UV-Vis absorption spectra of DPBF in a DMSO solution of complex **4** under O<sub>2</sub> atmosphere (Irradiation at  $\lambda_{irr} = 510$  nm). (D-E) The corresponding  $\ln(A_0/A_t)$

plots for the absorption at  $\lambda_{\text{abs}} = 418$  nm versus time. The rate constants of  $^1\text{O}_2$  generation for **4** were determined to be  $0.0191 (\pm 0.0009) \text{ s}^{-1}$ .

## Section D. Stability, Bio-Imaging, Cellular Uptake and Photodynamic Therapy

**1. Stability of metallacycle 2 in aqueous media.** The stability experiment was performed by measuring the changes in the UV-Vis spectra of metallacycle **2** in aqueous solutions at different pH conditions ( $c = 10 \mu\text{M}$ ) for 24 h using Perkin-Elmer Lambda 950 spectrometer. Different pH values adjusted by phosphate-buffered saline (PBS) were used to simulate the physiological condition ( $\text{pH} = 7.4$ ), tumor microenvironment ( $\text{pH} = 6.8$ ) and lysosome environment ( $\text{pH} = 5.3$ ), respectively.

**2. Cell culture and MTT assay:** Human cervical cancer cell lines (HeLa and Siha) and human normal cervical immortalized squamous cell line (Ect1/E6E7) used in this study were purchased from American Type Culture Collection (ATCC, Manassas, VA). The cells were exposed with different concentration of ligand **1**, metallacycle **2**, ligand **3**, complex **4** and  $\text{BpyPd}(\text{NO}_3)_2$  for 6 h, and then irradiated with or without light from a light-emitting diode (LED, 560 nm) with different doses at  $0.1 \text{ W/cm}^2$  or  $0.15 \text{ W/cm}^2$  for 2 min. The cells were incubated for another 24 h, and investigated the cell viability by MTT assay.<sup>[S7]</sup>

**3. Flow Cytometric Analysis:** Flow cytometry was used to examine the anticancer mechanisms of metallacycle **2** triggered by PDT. Briefly, HeLa cells ( $2 \times 10^4$  cells/mL, 6 mL) were seeded in 6 cm petri dish and attached for 24 h. Then the cells were incubated with metallacycle **2** at  $5 \mu\text{M}$  or  $10 \mu\text{M}$  for 6 h, then the cells were irradiated with LED (560 nm) at  $0.15 \text{ W/cm}^2$  for 2 min. The treated cells were incubated for another 24 h, and then collected, fixed with 75% ethanol solution for 2 h in  $-20 \text{ }^\circ\text{C}$ , and stained with PI in darkness at room temperature for 1 h. Then the stained cells were analyzed on Beckman CytoFLEX S flow cytometer.<sup>[S8]</sup>

**4. Measurement of singlet oxygen generation ( $^1\text{O}_2$ ) in HeLa cells triggered by metallacycle 2 and PDT:** The  $^1\text{O}_2$  generation in HeLa cells triggered by metallacycle **2** and PDT detected by DPBF assay.<sup>[S9]</sup> Briefly, HeLa cells ( $1 \times 10^5$  cells/mL, 0.1 mL) were seeded in 96-well plates and attached for 24 h. The cells were stained with the probe of DPBF ( $20 \mu\text{M}$ ) for 1 h, and then added the different concentration of Ligand **1** or metallacycle **2** ( $2.5, 5, 10, 20 \mu\text{M}$ ). The 96-well plates were analyzed for  $^1\text{O}_2$  generation in the HeLa cells within 100 minutes using a cell imaging multi-

mode reader (Cytation 5, BioTek Instruments, Inc.) at excitation and emission wavelengths of 410 and 484 nm, respectively. After 100 minutes, the cells were irradiated with LED (560 nm) at 0.15 W/cm<sup>2</sup> for 2 min, and then continue examining the <sup>1</sup>O<sub>2</sub> generation in the HeLa cells for another 60 min.

**5. Real-time living cell imaging:** Real-time observation of the cellular uptake and localization of Ligand **1**, metallacycle **2** and BpyPd(NO<sub>3</sub>)<sub>2</sub> were monitored by living cell imaging. Briefly, HeLa cells (8×10<sup>4</sup> cells/mL, 2 mL) were seeded in 35 mm Confocal dishes with coverglass bottom and attached for 24 h. The cells were stained with Hoechst 33342 for 0.5 h, and added with 10 μM of ligand **1**, metallacycle **2**, ligand **3**, complex **4** and BpyPd(NO<sub>3</sub>)<sub>2</sub> in the cells, respectively. After incubated with drugs for 6 h, 12 h and 24 h, the cells images were captured with fluorescence microscope. The cells also collected with pancreatin and analyzed the cellular uptake on Beckman CytoFLEX S flow cytometer with channel of PE.

**6. Cell distribution of metallacycle 2:** HeLa cells (8×10<sup>4</sup> cells/mL, 2 mL) were seeded in 35 mm confocal dishes with coverglass bottom and attached for 24 h. The cells were stained with Phalloidin green for 2 h and Hoechst 33342 for 0.5 h, and then treated with 10 μM of metallacycle **2** and incubated for another 12 h or 24 h. After washing with PBS twice, cell images were captured with z-stack mode by a confocal fluorescence microscope (ZEISS LSM800).

**7. Cell localization of metallacycle 2:** HeLa cells (8×10<sup>4</sup> cells/mL, 2 mL) were seeded in 35 mm Confocal dishes with coverglass bottom and attached for 24 h. The cells were stained with Lyso-Tracker green for 2 h and Hoechst 33342 for 0.5 h, and then treated with 10 μM of metallacycle **2** and incubated for another 12 h or 24 h. After washing with PBS twice, cell images were captured with z-stack mode by a confocal fluorescence microscope (ZEISS LSM800). The colocalization of metallacycle **2** and lysosome were analyzed with Imaris.

**8. *In vivo* fluorescence imaging of metallacycle 2:** The HeLa xenografts nude mice were intravenously injected with 2 mg/kg of metallacycle **2**, then anesthetized and monitored using a fluorescence imaging system (Night OWL II LB 983) at different time points (0, 8, 12, 24, 48 and 72 h). After injection for 48 and 72 h, the main organs of heart, liver, spleen, lungs, kidney and tumor of each group were taken out and the fluorescence distribution also investigated using the fluorescence imaging technique. The 8-μm sections of tumor tissues were obtained and stained the nucleus with Hoechst 33342 for 0.5 h. The red fluorescence of metallacycle **2** in tumor sections was captured with fluorescence microscope. All of the animal studies were performed in strict accordance with the national guidelines for the care and use of laboratory animals (Laboratory

animal-Guideline for ethical review of animal welfare. GB/T 35892-2018) and was approved by the Animal Experimentation Ethics Committee of Jinan University (Guangzhou, China).

**9. *In vivo* biocompatibility and safety evaluation of metallacycle 2:** 8-week-old BALB/c mice were randomly separated into three groups (10 mice/group), and then intravenously injected with saline, metallacycle **2** or complex **4** (2 mg/kg, injection volume: 100  $\mu$ L). After 3 days, the whole blood samples (about 500  $\mu$ L) were collected in EDTA anticoagulant tubes from the retroorbital plexus of the mouse eye (one half mice). The blood routine examination was performed on automatic hematology analyzer for animal (Mindray, BC-2800vet). The blood samples were also collected from the other half mice and centrifuged at 3000 rpm to obtain the serum and performed the hematological analysis. Biochemical parameters including ALT (alanine aminotransferase), AST (aspartate transaminase), ALB (albumin), TP (total protein), UREA (urea), BUN (blood urea nitrogen), CREA (creatinine), UA (uricacid). The major organs of mice including heart, liver, spleen, lung and kidney, were obtained and performed the H&E staining to conduct the Pathological analysis.

**10. *In vitro* cellular uptake of metallacycle 2:** Different chemical endocytosis inhibitors were performed to investigate the cellular uptake behavior of metallacycle **2**.<sup>[S6]</sup> Briefly, HeLa cells ( $8 \times 10^4$  cells/mL, 0.1 mL) were seeded in 96-well plates and attached for 24 h. The cells were pre-treated with  $\text{NaN}_3$  (10 mM), chlorpromazine (10  $\mu$ g/mL), sucrose (0.45 M), dynasore (1.6 mM), nystatin (10  $\mu$ g/mL) and incubated at 4  $^\circ\text{C}$  for 1 h. HeLa cells were then incubated with 10  $\mu$ M of metallacycle **2** for different periods of time at 37  $^\circ\text{C}$  or 4  $^\circ\text{C}$ . The control groups were incubated with metallacycle **2** at 37  $^\circ\text{C}$  only. At the end of the incubation, the medium was removed from the wells and the cells were rinsed three times with cold PBS to remove the particles outside the cells. After that, 100  $\mu$ L of 0.5% Triton X-100 in 0.2 M NaOH solution was added to lyse the cells. A standard curve for metallacycle **2** was constructed by suspending different concentrations in the same plate. The 96-well plates were analyzed with fluorescence intensity of metallacycle **2** by a cell imaging multi-mode reader (Cytation 5, BioTek Instruments, Inc.) at excitation and emission wavelengths of 550 and 627 nm, respectively. The uptake of metallacycle **2** in HeLa cells was calculated from the standard curve and expressed as the quantity ( $\mu$ g) per  $10^6$  cells.

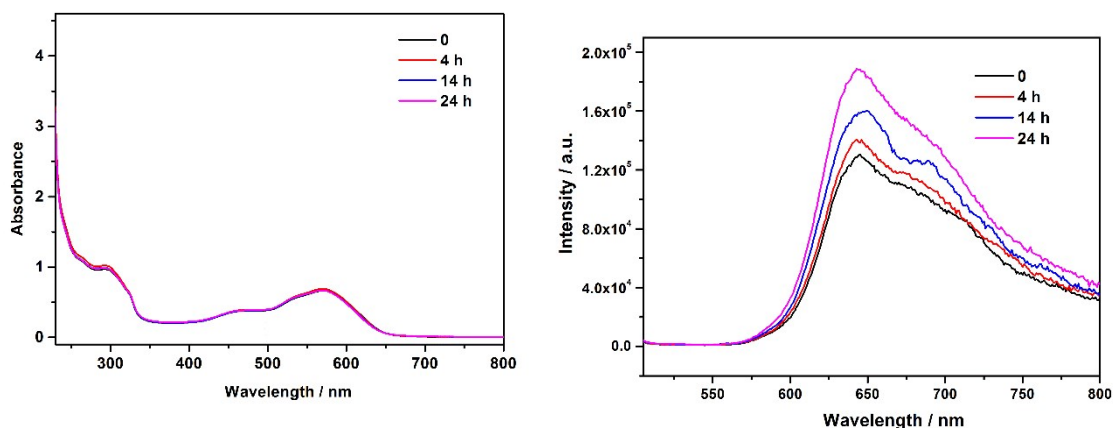


**Figure S49** Changes in UV-Vis spectra (left) and emission spectra (right) of metallacycle **2** versus time in PBS buffer at pH =7.4 ( $c = 10 \mu\text{M}$ ).

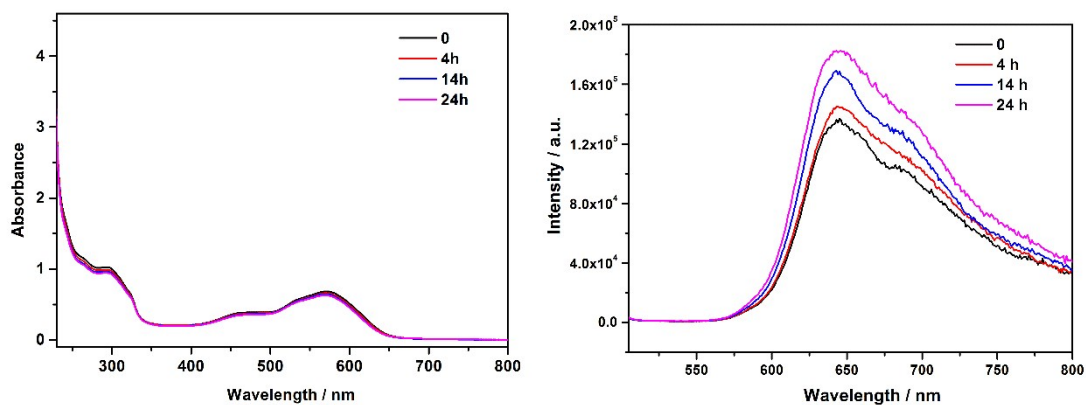


**Figure S50** Changes in UV-Vis spectra (left) and emission spectra (right) of metallacycle **2** versus time in PBS buffer at pH =6.8 ( $c = 10 \mu\text{M}$ ).

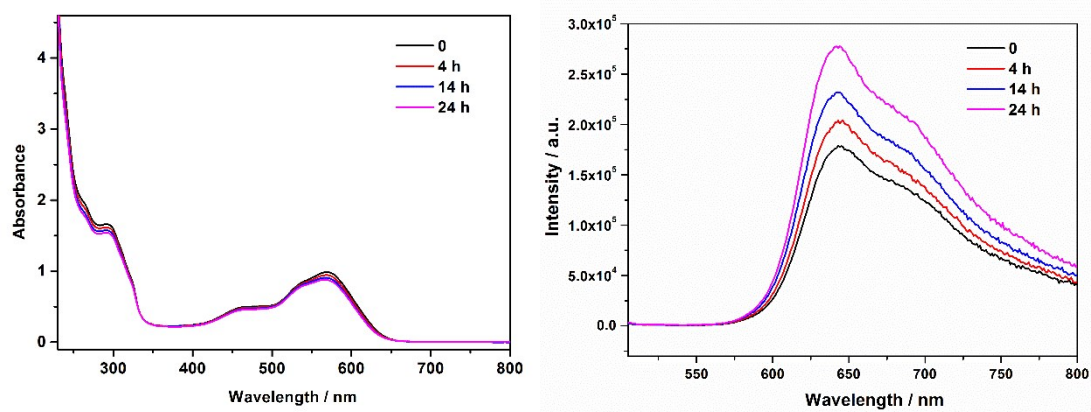


**Figure S51** Changes in UV-Vis spectra (left) and emission spectra (right) of metallacycle **2** versus time in PBS buffer at pH =5.3 ( $c = 10 \mu\text{M}$ ).

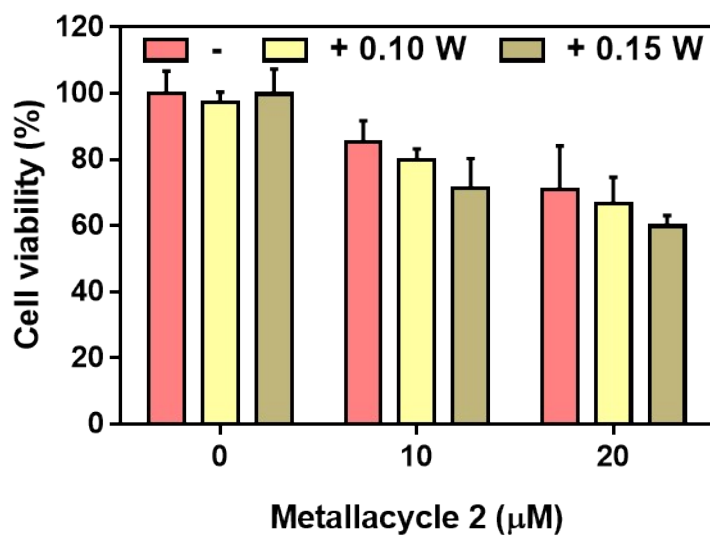


**Figure S52** Siha cell viability of metallacycle **2** combined with PDT. The cells were incubated with metallacycle **2** for 24 h.

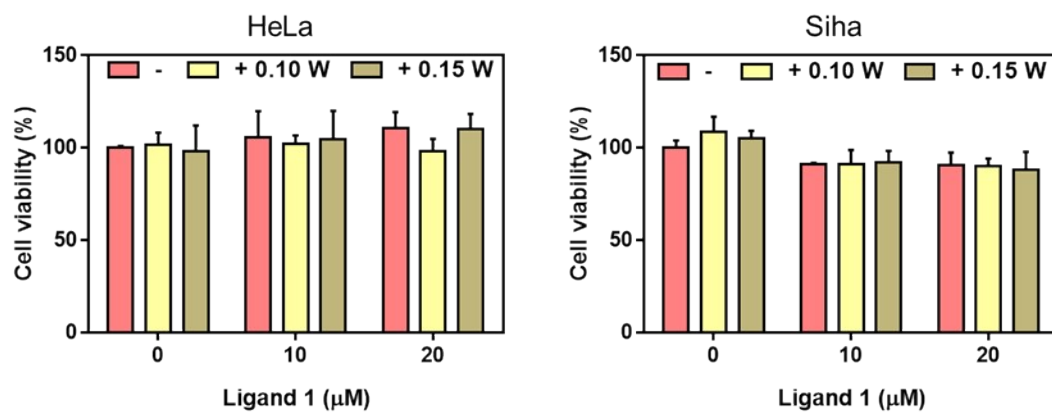


**Figure S53** Cell viability of ligand **1** combined with PDT. The cells were incubated with ligand **1** for 24 h.

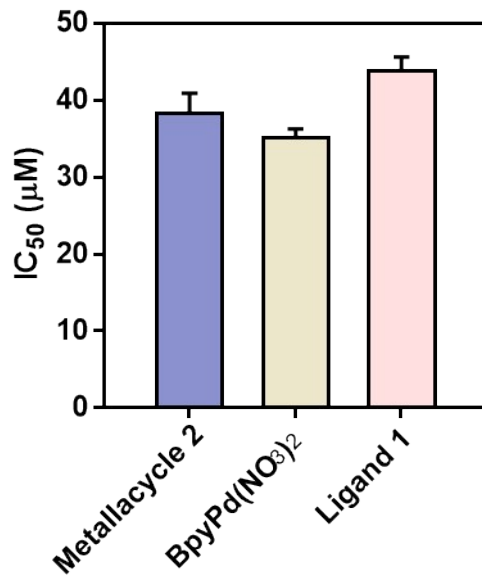


**Figure S54** IC<sub>50</sub> values of ligand 1, BpyPd(NO<sub>3</sub>)<sub>2</sub> and metallacycle 2 against normal human cervical immortalized squamous cells (Ect1/E6E7). The cells were treated with these molecules for 72 h.

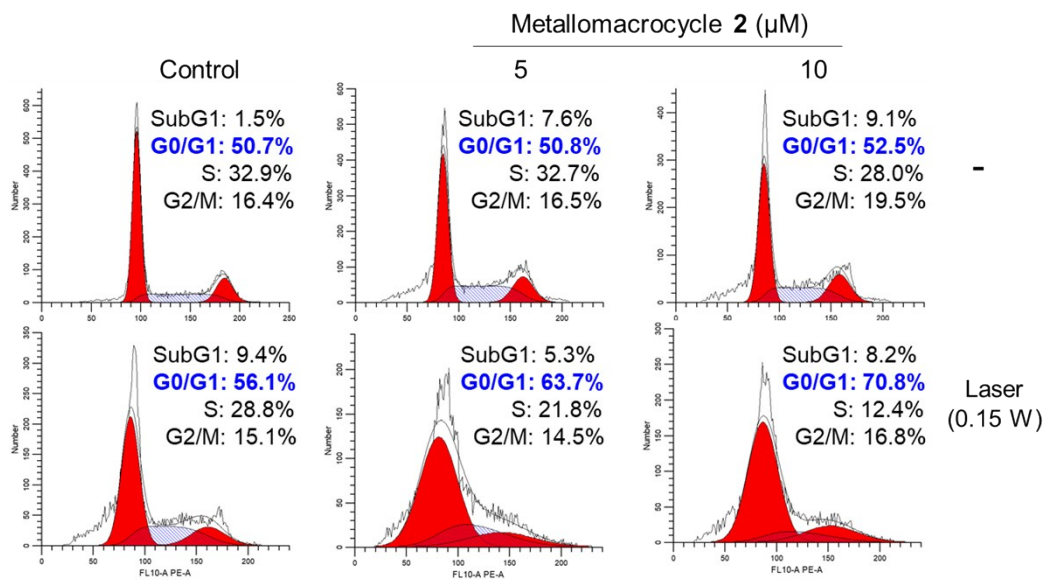


**Figure S55** Metallacycle **2** enhanced PDT-induced cell cycle arrest in HeLa cells. The cells were incubated with metallacycle **2** for 24 h.

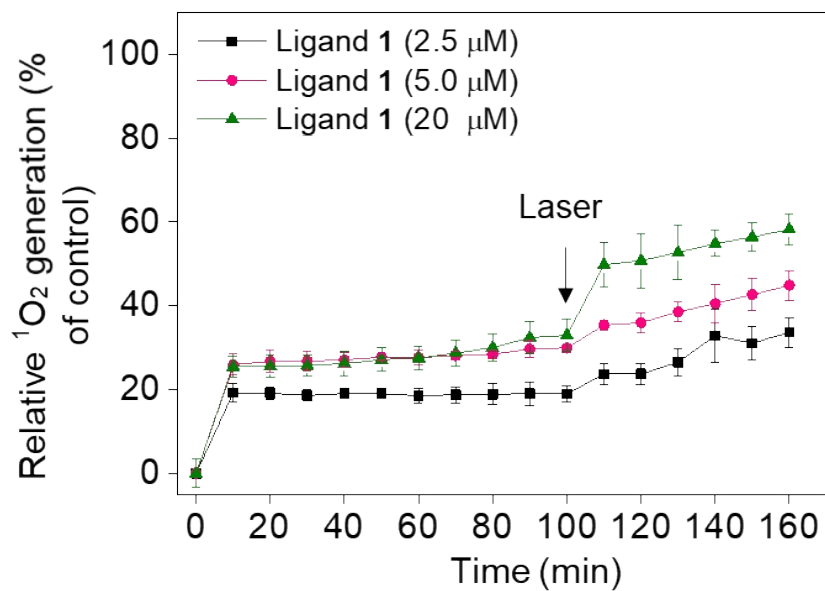


**Figure S56** Concentration effect of ligand **1** on PDT-induced singlet oxygen overproduction in HeLa cells.

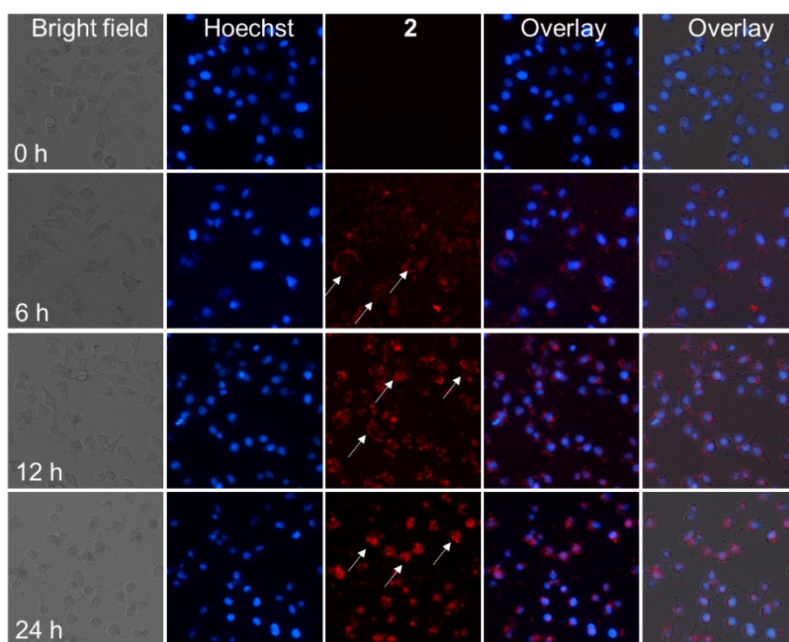


**Figure S57** Intracellular trafficking of metallacycle **2** (10  $\mu$ M) in HeLa cells.

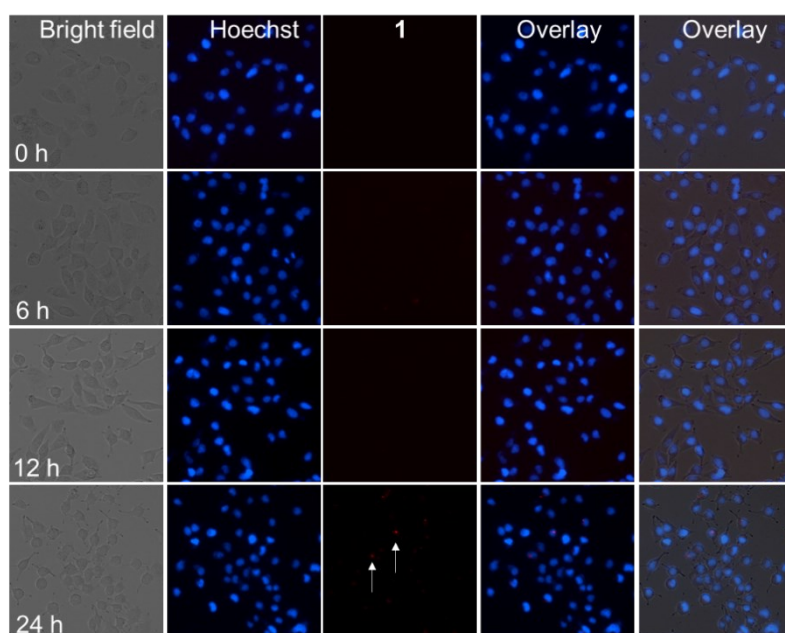


**Figure S58** Intracellular trafficking of ligand **1** (10  $\mu$ M) in HeLa cells.

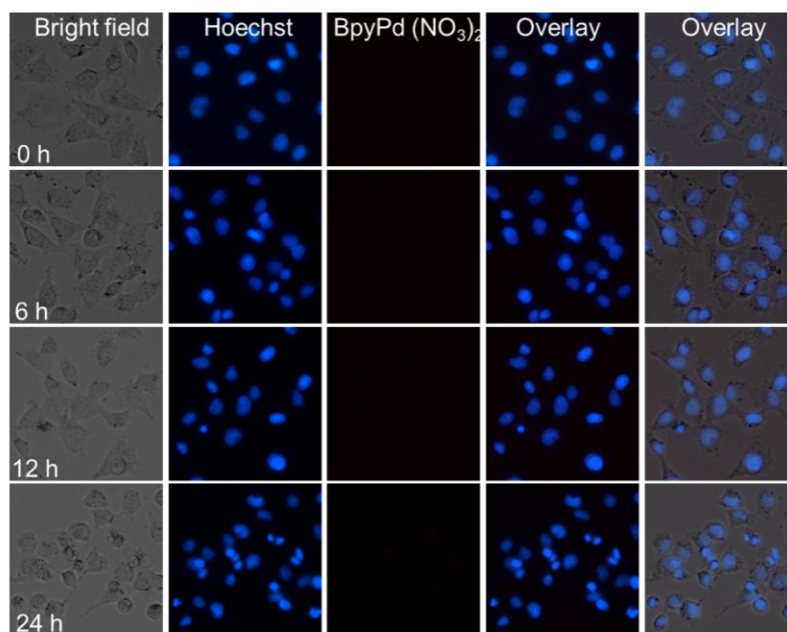


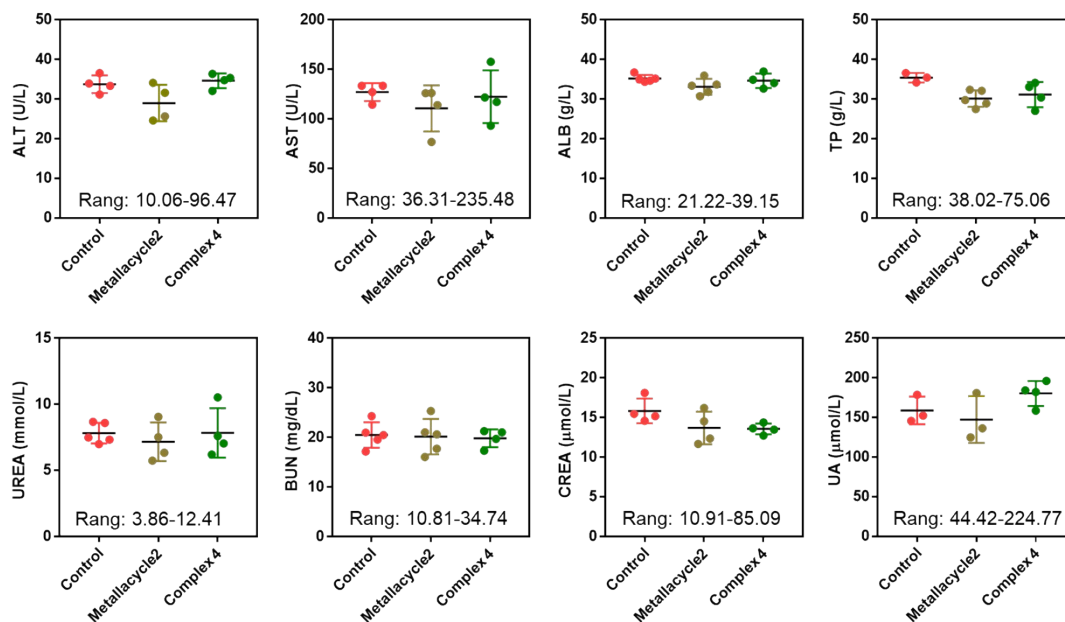
**Figure S59** Intracellular trafficking of BpyPd(NO<sub>3</sub>)<sub>2</sub> (10 μM) in HeLa cells.

**Table S3** Blood routine examination of mice treated with metallacycle **2** or complex **4**. The mice were intravenously injected with 2 mg/kg of metallacycle **2** or complex **4** for 3 days.

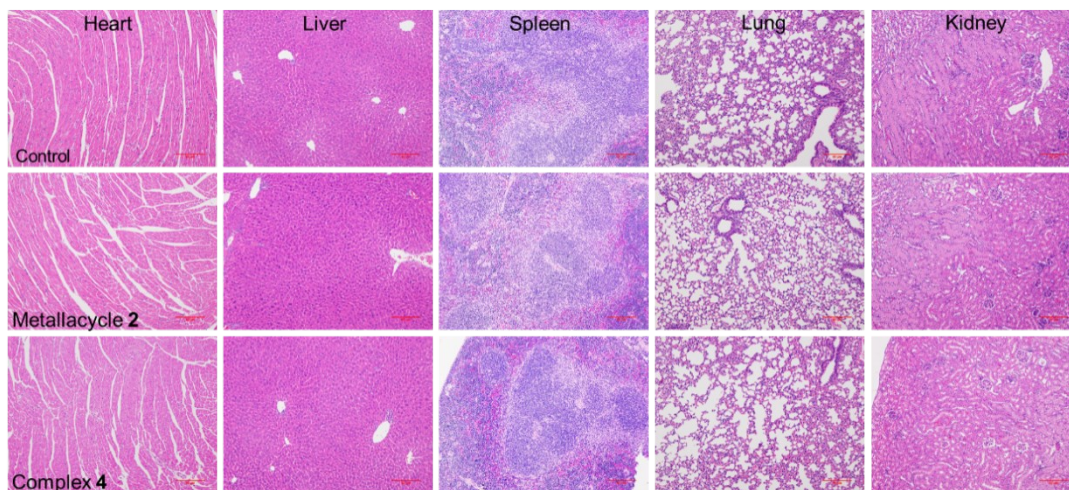
Parameter	Control	Metallacycle <b>2</b>	Complex <b>4</b>	Unit	Standard
WBC	5.4±1.31	5.22±0.72	5.3±0.83	10 <sup>9</sup> /L	0.8-6.8
Lymph#	3.77±0.95	3.95±0.44	4.06±0.62	10 <sup>9</sup> /L	0.7-5.7
Mon#	0.2±0.13	0.2±0.08	0.16±0.05	10 <sup>9</sup> /L	0.0-0.3
Gran#	1.43±0.29	1.07±0.22	1.08±0.23	10 <sup>9</sup> /L	0.1-1.8
Lymph%	69.77±1.75	75.72±2.01	76.26±2.01	%	55.8-90.6
Mon%	3.57±0.29	3.8±0.45	3.56±0.58	%	1.8-6.0

Gran%	26.67±2.03	21.33±0.74	20.18±2.03	%	8.6-38.9
RBC	8.49±0.48	7.78±0.58	8.44±0.47	10 <sup>12</sup> /L	6.36-9.42
HGB	125.67±6.81	117.75±10.81	130.8±6.06	g/L	110-143
RDW	16.6±0.17	16.03±0.35	16.24±0.55	%	13-17
PLT	1306.5±500.89	1293±468.62	1465±147.02	10 <sup>9</sup> /L	450-1590

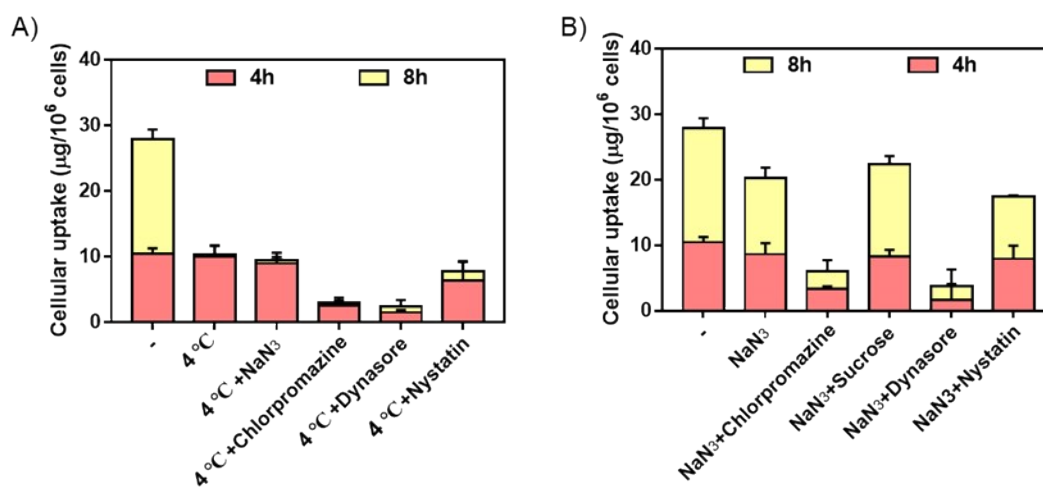
WBC: White Blood Cell, Lymph#: Lymphocyte, Mon#: Monocyte, Gran#: Granulocyte, Lymph%: Lymphocyte Percentage, Mon%: Monocyte Percentage, Gran%: Granulocyte Percentage, RBC: red blood cell, HGB: hemoglobin, RDW: Coefficient of variation of erythrocyte distribution width, PLT: platelet.



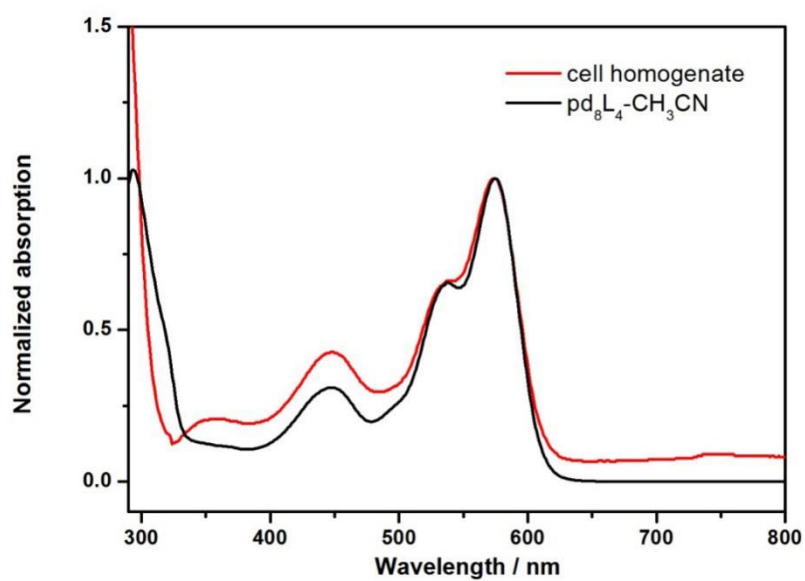
**Figure S60** Hematological analysis of mice treated with treated with metallacycle 2 or complex 4 for 3 days.



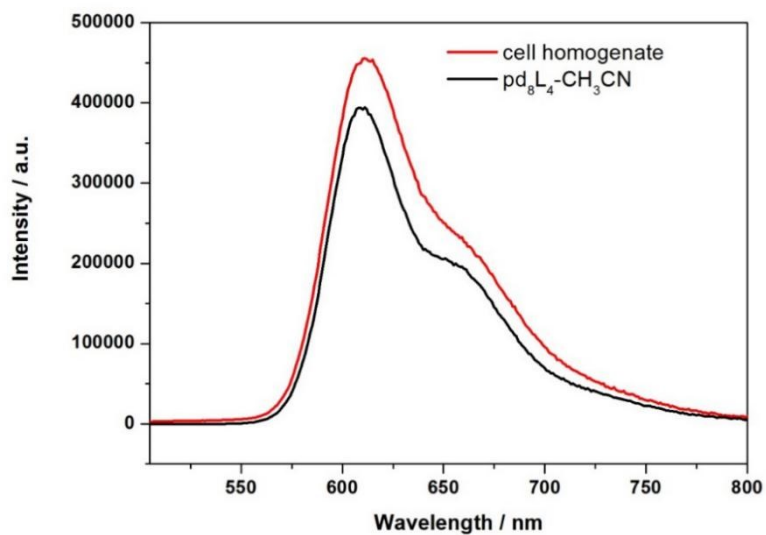
**Figure S61** H&E staining of the heart, liver, spleen, lung, and kidney after treatment with metallacycle **2** or complex **4** for 3 days (Scale bars are 50  $\mu\text{m}$ ).



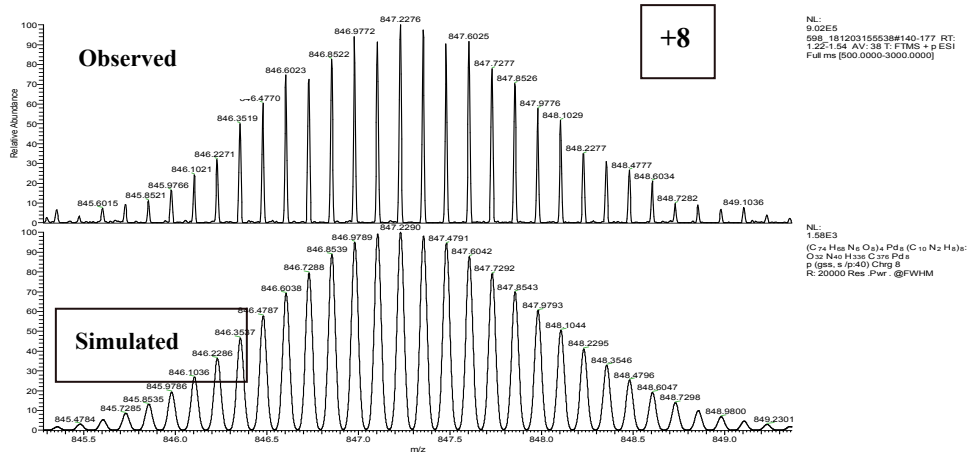
**Figure S62** Intracellular uptake of metallacycle **2** in HeLa cells after pretreated with different endocytosis inhibitors. HeLa cells were pretreated with various endocytosis inhibitors for 1 h and then incubated with 10  $\mu\text{M}$  of metallacycle **2** for different periods of time at 37 °C or 4 °C. The control groups were incubated with metallacycle **2** only at 37 °C.



**Figure S63** Changes in UV-Vis spectra of metallacycle **2** extracted from cell lysate after incubated with HeLa cells for 24 h.



**Figure S64** Changes in emission spectra of metallacycle **2** extracted from cell lysate after incubated with HeLa cells for 24 h.



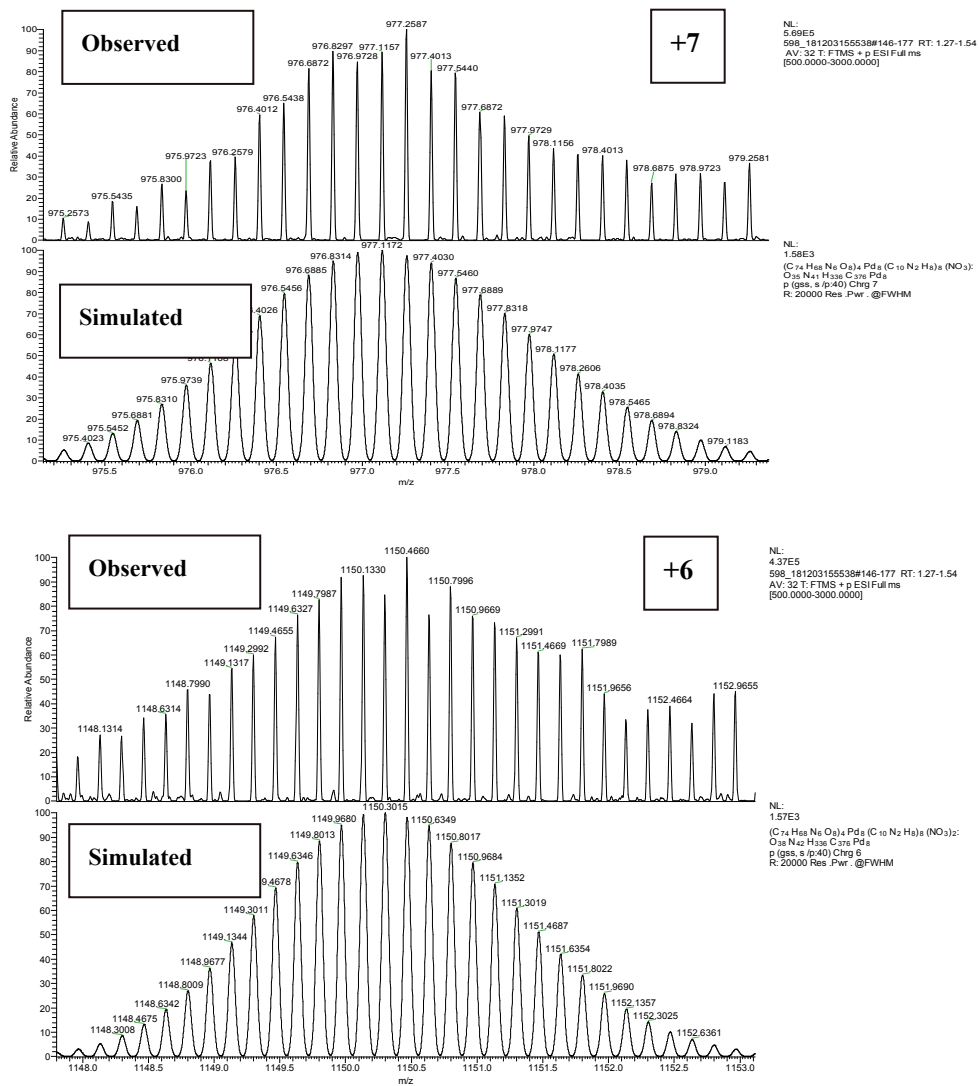
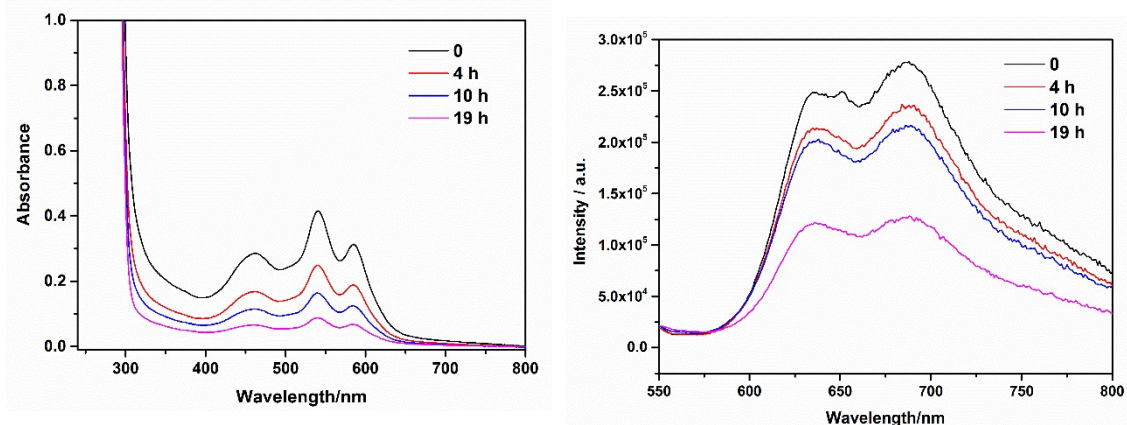
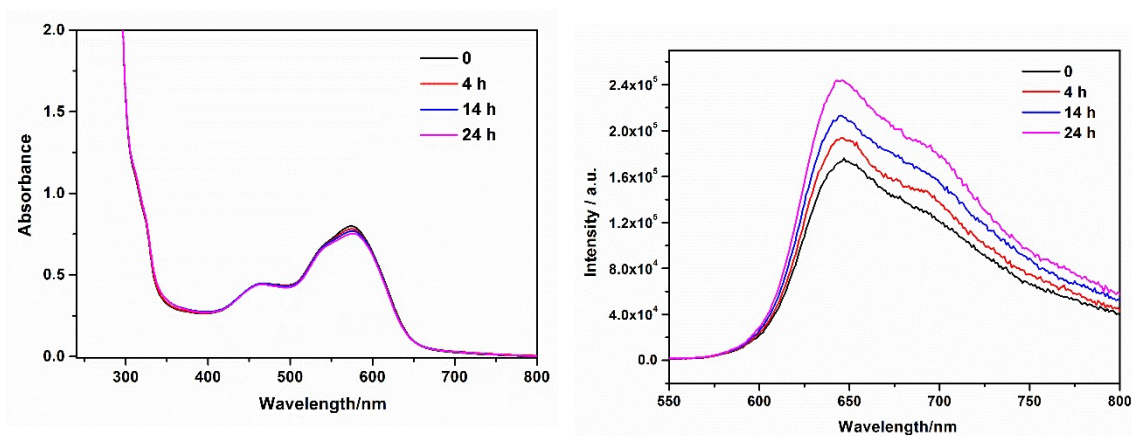


Figure S65 ESI-MS spectra for metallacycle 2 in water at pH = 5.3 containing lysozyme after 2 h.



**Figure S66** Changes in UV-Vis absorption (left) and emission spectra (right) of ligand **1** versus time in PBS buffer at pH = 5.3 containing lysozyme ( $c = 20 \mu\text{M}$ ).



**Figure S67** Changes in UV-Vis absorption (left) and emission spectra (right) of metallacycle **2** versus time in PBS buffer at pH = 5.3 containing lysozyme ( $c = 10 \mu\text{M}$ ).

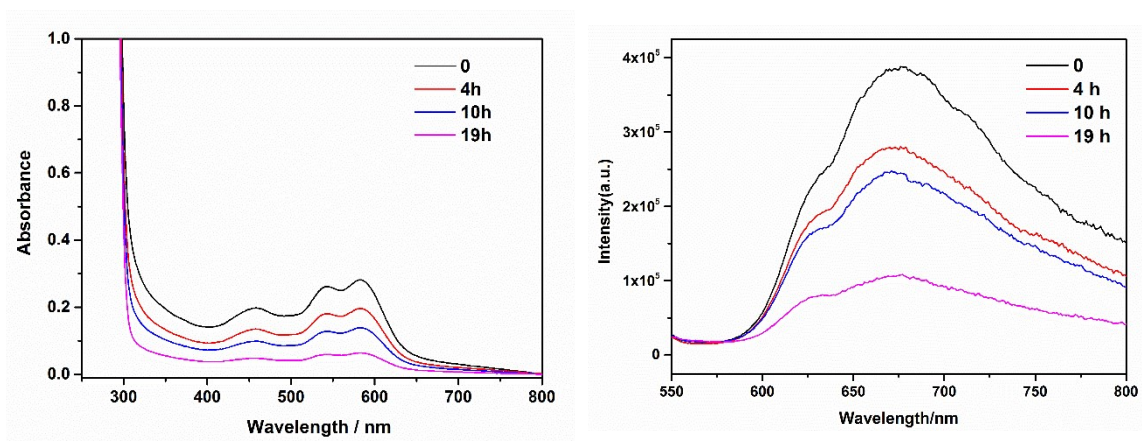


**Figure S68** Changes in UV-Vis absorption (left) and emission spectra (right) of ligand **3** versus time in PBS buffer at pH = 5.3 containing lysozyme (c = 20  $\mu$ M).

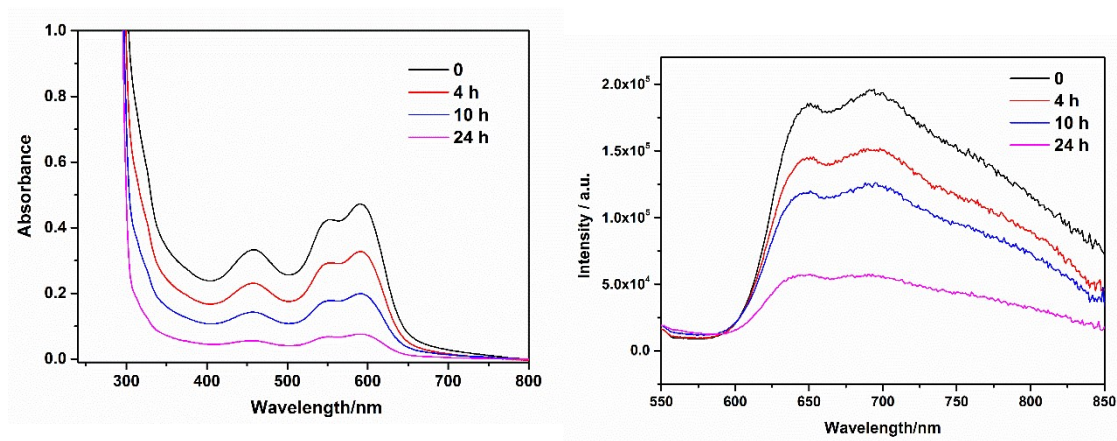


**Figure S69** Changes in UV-Vis absorption (left) and emission spectra (right) of complex **4** versus time in PBS buffer at pH = 5.3 containing lysozyme (c = 20  $\mu$ M).

## Section E. References

- S1. Gong, H. X.; Cao, Z.; Li, M. H.; Liao, S. H.; Lin, M. J. *Org. Chem. Front.* **2018**, *15*, 2296-2302.
- S2. Ke, H;Weng, L-J; Chen, S-Y; Chen, J-Z; Lin, M-J. *Dyes Pigments.* **2015**, *113*, 318-324.
- S3. Agilent Technologies,CrysAlisPro v. 1.171.36.28, **2013**.
- S4. Sheldrick, G. M. *Acta Crystallogr. Sect. A* **2008**, *64*, 112-122.

- S5. Spek, A. L.; *J. Appl. Crystallogr.* **2003**, *36*, 7-13.
- S6. (a) De Mello, J. C.; Wittmann, F. H.; Friend R. H. *Adv. Mater.* **1997**, *9*, 230-232; (b) Lv, R.; Yang, F.; Jiang, X.; Hu, B.; Zhang, X.; Chen, X.; Tian, J. *J. Lumin.* **2020**, *220*, 116974.
- S7. Huang, Y.; He, L.; Liu, W.; Fan, C.; Zheng, W.; Wong, Y. S.; Chen, T. *Biomaterials* **2013**, *34*, 7106-7116.
- S8. Li, Y.; Li, X.; Zheng, W.; Fan, C.; Zhang, Y.; Chen, T. *J. Mater. Chem. B* **2013**, *1*, 6365–6372.
- S9. Huang, H.; He, L. Z.; Zhou, W. H.; Qu, G. B.; Wang, J. H.; Yang, N.; Gao, J.; Chen, T. F.; Chu, P. K.; Yu, X. F. *Biomaterials* **2018**, *171*, 12-22.